ANNALS OF THE NEW YORK ACADEMY OF SCIENCES

VOLUME 62, ART. 20 PAGES 449-502

Editor
ROY WALDO MINER

AN X-RAY STUDY OF URANINITE

BY
WILLIAM J. CROFT

NEW YORK
PUBLISHED BY THE ACADEMY
February 10, 1956

ANNALS OF THE NEW YORK ACADEMY OF SCIENCES

VOLUME 62, ART. 20 PAGES 449-502

February 10, 1956

Editor

ROY WALDO MINER

AN X-RAY STUDY OF URANINITE

BY

WILLIAM J. CROFT

Massachusetts Institute of Technology,
Lincoln Laboratory, Lexington, Mass.

CONTENTS

AN X-RAY STUDY OF URANINITE*

BY

WILLIAM J. CROFT

X-ray Texture of UO_2

Introduction. This study is concerned with the diffraction of monochromatic X rays by the naturally occurring forms of uranium oxides. The oxide of uranium found in greatest abundance, as a mineral, is the face-centered cubic (fluorite type) form of uranium dioxide. The first part of this paper is concerned with the crystal textures of the mineral forms of this oxide, and the second part is an examination of the powder X-ray diffraction data from various samples of natural and artificial UO_2.

UO_2 almost always occurs in nature in a crystalline form. This may not always be indicated by the morphology of the mineral, but may be observed by its diffraction of X rays. The so-called "amorphous compound UO_3" is often reported in chemical analyses of uraninite. It is problematical whether this oxide exists in nature. All of the uranium-oxygen compounds are known to be nonstoichiometric. The mineral compound UO_2 is often found with considerably more than its formula amount of oxygen. To balance this excess, some of the uranium is in a +6 valence state. The cubic face centered structure is still maintained (up to the point $UO_{2.3}$). Whether the structure has vacant uranium sites or only an excess of oxygen atoms is still an unresolved problem which at times borders on semantics. The introduction of oxygen into the stoichiometric UO_2 structure decreases the size of the unit cell and creates a disordered structure. These effects are discussed in the later part of the paper.

Uraninite and pitchblende. Since this paper is concerned with the naturally occurring oxides, it would be well to examine the variety of mineral forms which the oxides may assume. In describing these, the terms uraninite and pitchblende have been loosely employed throughout the literature.

There has been much discussion concerning proper usage for the terms uraninite and pitchblende. The two have been distinguished in various ways, which include: mode of aggregation (Rogers, 1947); chemical composition (Ellsworth, 1932); origin (Brooker and Nuffield, 1952); and the extent of alpha activity (Yagoda, 1946). From the standpoint of lattice development, uraninite is face-centered cubic with a cell edge dimension that varies but is on the order of 5.47 Å. (Palache *et al.*, 1944). Pitchblende is structurally the same, and no consistent difference in cell dimensions appears to exist that distinguishes the two.

*This paper describes part of the results of research performed at Columbia University, New York, N. Y., under Contract No. AT(30-1)-702 with the United States Atomic Energy Commission, Washington, D. C.

Rogers considered pitchblende to be a massive mineraloid and reserved the name uraninite for the crystalline equivalent. The term mineraloid, however, originated (Niedzwiedzki, 1909) prior to the use of X rays for the determination of the crystallinity of finely divided opaque matter.

Chemical composition has been a factor used at times to distinguish uraninite from pitchblende. As stated by Ellsworth (1932, p. 131), uraninite invariably contains ThO_2 with a small percentage of the rare earths, while pitchblende contains no thorium, or only traces of it, and little or no rare earths. Uraninite, when crystallized, is believed to be primarily UO_2, although at times it may contain up to 12 per cent ThO_2 substituted in the lattice. A number of analyses of uraninite as listed by Palache, Berman, and Frondel (1944), however, are essentially free from thorium; hence the distinction between uraninite and pitchblende on the basis of the presence or absence of thorium appears tenuous.

It has been assumed by some, on chemical grounds, that uraninite, when originally formed, was UO_2, while pitchblende was U_3O_8. Katz and Rabinowitch (1951), Ellsworth (1932), and Yagoda (1946) consider pitchblende to be U_3O_8, although X-ray data on minerals fail to show the structural difference that this distinction would imply.

Yagoda (1946) has established groups of radioactive minerals on the bases of relative alpha-activity. Uraninite falls into the most active group, but different samples of pitchblende are found in several groups. The variation in alpha-activity may be caused by leaching and variation in the purity of individual samples.

Brooker and Nuffield (1952) and Ellsworth (1932) distinguish between pitchblende and uraninite on the basis of origin, uraninite being pegmatitic, and pitchblende of vein origin. Origin, as a basis for distinction, is ordinarily used in descriptions of Canadian occurrences as a prospecting aid. It is open to question as a criterion for technical distinction, since crystals of uraninite may be found imbedded in a mass of pitchblende, as at Shinkolobwe in the Belgian Congo. It is possible that the crystals originated in a pegmatite, but they show no signs of transportation, being euhedral cubes.

Kerr (1950) has pointed out that it is not necessarily essential to make a distinction. This follows the usage of Dana's *System of Mineralogy* (1944). The British generally follow the same usage. Davidson and Bowie (1951) use uraninite "in a comprehensive sense inclusive of the amorphous form 'pitchblende.' "

The above is only a cross section of the many references to the nature of uraninite and pitchblende.

X-ray examination. X-ray examination of many specimens of naturally

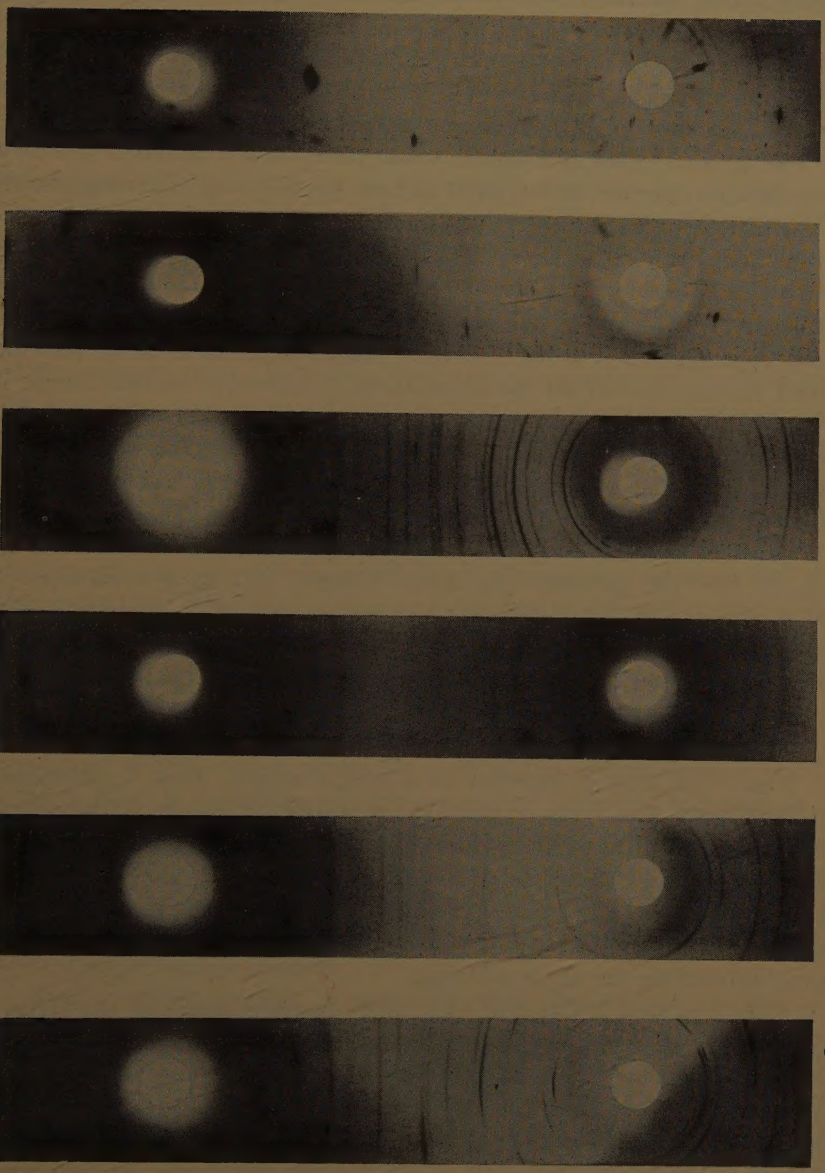

PLATE 1. Laue-type diagrams of pitchblende and uraninite.

occurring UO_2 has been made in the following manner. A chip of mineral about 0.2 mm. in size is placed on a fibre with Duco cement and mounted at the center of a 57-mm. diameter Debye-Scherrer camera. It is exposed to unfiltered copper radiation (40 kilovolts and 18 milliamperes) for approximately two hours, remaining stationary during the exposure.

Two general types of diagrams result from these exposures. One is a Debye-Scherrer picture with typical uniform powder rings. This represents the diffraction of the characteristic radiation by randomly oriented crystallites less than 10^{-3} cm. in dimension. The other type of diagram is one which resembles a Laue photograph. Weak spots result from the diffraction of the white radiation by a large crystal. Occasionally a strong spot appears if a set of crystal planes happens to be in just the correct position to diffract the characteristic radiation. On this basis, it is possible to distinguish between two types of material and arrive at a useful distinction for each. The term uraninite might be reserved for naturally occurring UO_2 having megascopic crystal size and often showing external crystal form. The name pitchblende, on the other hand, might be applied to material composed of randomly oriented crystallites on the order of 10^{-3} cm. in size. The latter material may have a massive or colloform external form. Observations fail to disclose a gradation between the microcrystalline material and macrocrystals. Observations have not been extended to include the natural black uranium powders or sooty ores. Six typical films are reproduced on PLATE 1. In all of the films, the back reflection region is to the left.

Film 1 is from a fragment of a single crystal from Shinkolobwe, Belgian Congo. The spots on the film are diffracted images of the source collimator due to the white radiation. One spot is particularly intense, due to the chance diffraction from a set of crystal planes by the characteristic radiation. The faint curves and streaks in the front reflection region are probably due to tiny crushed fragments on the surface of the sample diffracting the white radiation.

Film 2 is from a fragment of a large massive chunk of UO_2 from a pegmatite in Parahyba, Brazil. The sample is thoroughly veined by alteration and secondary minerals. No external crystal form is evident on macroscopic observation, but the presence of strong spots on the film indicates a strong orientation on a large scale. The fact that most of the spots show streaks or are smeared may be due to disorder of the crystal structure by alteration.

Film 3 is from a chip of massive vein material from Johanngeorgenstadt, Saxony, East Germany. The film appears as a typical Debye-Scherrer photograph, although it is made from a nonrotating, unground fragment. The lines are continuous and nonspotty. These indicate the

sample to be composed of a randomly oriented aggregate of crystallites 10^{-3} cm. in size or smaller. This is a typical pitchblende pattern.

Film 4 is made from a grain separated from a crushed sample of a brecciated vein from Marysvale, Utah. This is seen to be a pitchblende. The diffuseness of the lines indicates either a very small particle size (less than 10^{-5} cm.), or disorder in the structure, or both. The inner line is due to an unidentified impurity intimately mixed with the sample.

Film 5 is made from a chip of material from the Rickards Mine, Gilpin Co., Colo. The sample is from a vein about 1 cm. wide which is filled solidly with hard, compact pitchblende.

Film 6 is made from a botryoidal chip of pitchblende from Great Bear Lake, Northwest Territories, Canada. Films 5 and 6 show incomplete Debye-Scherrer rings, indicating that random orientation is incomplete. The chip may have been slightly too large, and the incompleteness may be an absorption effect, since other chips from the same samples give complete patterns.

In general, certain effects may be noted on all of these films. Since the samples have an extremely high absorption coefficient, the back reflection regions are most darkened due to fluorescent radiation and general scattering. The front reflections are due to diffraction from a thin outer edge of the sample. Pitchblende films have more over-all darkening than those of uraninite, due to the continuous diffraction of the white radiation by the randomly oriented crystallites. A sharp shadow may be seen on Film 6. This is due to the diffraction and scattering from a thin appendage of the sample, while the bulk of the sample casts a shadow in the X rays. It should be noted that the line positions and relative intensities in these pitchblende films are not comparable with the usual Debye-Scherrer films because of irregular sample shape and centering. Films 5 and 6 suggest the diagrams produced by stretched fibers and lead to a more detailed investigation of the textures of the materials which produce such a diagram.

Texture investigations. It was found that the diagrams showing preferred orientation are produced by botryoidal pitchblende, as well as some vein types. These were investigated by the use of a flat cassette camera from which full Debye-Scherrer rings could be examined in both the front and back reflection region. Some of the diagrams obtained are reproduced in PLATES 2, 3, and 4. The samples are mounted with Duco cement on a glass fiber that is placed on a goniometer mounting head. This head can be placed on a two-circle goniometer for orientation purposes and then transferred to the flat cassette camera with the sample intact. The films shown in PLATE 2 were made with the fine X-ray beam glancing across the surface of a botryoid of pitchblende from Great Bear

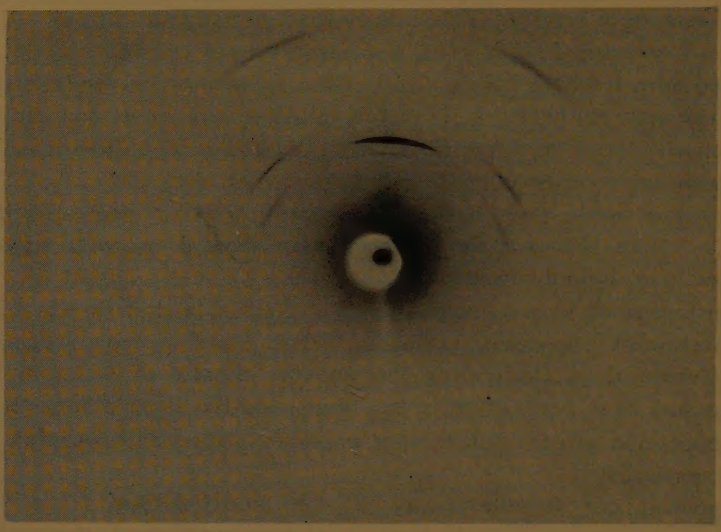

1

2

PLATE 2. X-ray texture of botryoidal pitchblende, Great Bear Lake, N. W. T., Canada.

Lake. Filtered copper radiation was used. The surface of the sample was in a horizontal position. It is observable from the film that certain crystallographic planes are strongly oriented. This is most evident in Film 1, the front reflection region. The film is easily indexed to determine the orientation. The diameter of each ring is measured and also the specimen to film distance. From this, the tangent of the Bragg angle can be computed. This is used to get the cosine value and is substituted in the equation for Bragg's law to determine the interplanar spacing responsible for each ring. Since the substance in question is cubic face centered, it is easy to assign indices to the various reflections on the basis of the multiplicity of the values of $\sin^2\theta$.

The strongest arc in the picture is the (111) reflection. Two weaker arcs of the same radius are seen to the left and right. The faint arc within the strong (111) arc is the reflection due to the Kβ component of the copper radiation. The next outer reflection is the (200) which gives arcs left and right of center but not in the center itself. This diagram closely resembles the type produced by fibers. The diagram produced by a truly parallel bundle of fibers shows the layer line arrangement of spots of a rotation diagram. As the parallelism decreases, the spots become arcs and, eventually, as the orientation becomes completely random, a Debye-Scherrer pattern of rings results. The diagram presented here indicates strong parallelism. The deviation from parallelism is due to the fact that the fibers are perpendicular to the curved surface of the botryoid. The position and great intensity of the (111) reflection shows that it is the plane perpendicular to the fiber axis. The multiplicity of similar planes resulting from the cubic symmetry causes the weaker (111) reflections on either side of the strong one. The diagram has a vertical line of symmetry, as would be expected, but horizontal symmetry is absent, since the lower reflections are completely absorbed. This material (UO_2) has an extremely high absorption coefficient for X rays. As will be seen in a later part of this paper, the diffraction effect illustrated here is produced by a tip of the curved surface 0.006 mm. in length.

It is the curvature of the surface containing the (111) planes that allows the maximum diffraction effect to take place, since so many of these planes will be in the optimum diffracting position. If the fibers were truly parallel to each other and perpendicular to the X-ray beam, diffraction could not take place from the (111) planes (those perpendicular to the fiber axis) because the angular condition of the Bragg equation would not be fulfilled.

The lower illustration in PLATE 2 is a photograph of the back reflections taken simultaneously with the front reflections of illustration 1. The Debye-Scherrer rings are more diffuse because they result from

diffraction of the entire portion of the beam which hits the specimen. This is in addition to the diffuseness resulting from the geometry of the line broadening. The shadow of the goniometer head on the film is caused by X-ray scattering from the direct beam trap. The rings are much more complete in this back reflection region because of the high multiplicity factor of some of the reflections, *e.g.* (622), (533), (620) each have multiplicity factors of 24, which means that, for each reflection, 24 planes of the same index but different position scatter cooperatively at the same Bragg angle.

The scatter of tiny sharp reflections on this back reflection region is due to minute admixed fragments of crystalline quartz.

An X-ray diagram (not illustrated) made with the beam perpendicular to the botryoid surface (in other words parallel to the fiber length) shows complete Debye-Scherrer rings. This is further evidence of the fibrous nature of this sample, and also indicates the random orientation (in a rotational sense) of the fiber axes with respect to one another.

The sample just described represents the filling of an open fracture or cavity by precipitation or crystal growth on the wall of the opening.

The first diagram on PLATE 3 was made from a sample taken from the edge of a narrow (1 cm.) vein of pitchblende from the Wood Mine, Gilpin Co., Colo. This diagram was taken with the X-ray beam parallel to the plane of the vein wall. This is the same type of diagram as that obtained from the botryoid of the Great Bear Lake sample. In this case, as in the previous one, the fiber axis is the pole of the (111) plane. The diagram taken with the beam perpendicular to the vein wall shows continuous Debye-Scherrer rings.

The lower diagram on PLATE 3 was taken from pitchblende from a thick vein filled with brecciated fragments of quartz and sulphides from Great Bear Lake. This diagram shows complete Debye-Scherrer rings. The same sample was X-rayed in four other orientations and, in all cases, the same type of diagram appeared. This is considered satisfactory evidence that a random orientation exists in this sample.

These diagrams are typical of many that have been taken. In the case of the botryoidal samples and in the case of thin veins, as well as in samples taken close to the vein wall of thick veins, this apparent fibrous structure is present, with the fiber axis being the pole of the (111) planes and the fibers having random rotation with respect to one another. On the basis of this type of diagram, the fibers are less than 10^{-3} cm. in diameter. It is not possible to tell directly if they have a circular cross-section, but they probably do not. The mechanism of growth appears to be a spreading out on a growth surface of the atoms occupying the (111) planes from a great many centers. Since the samples

1

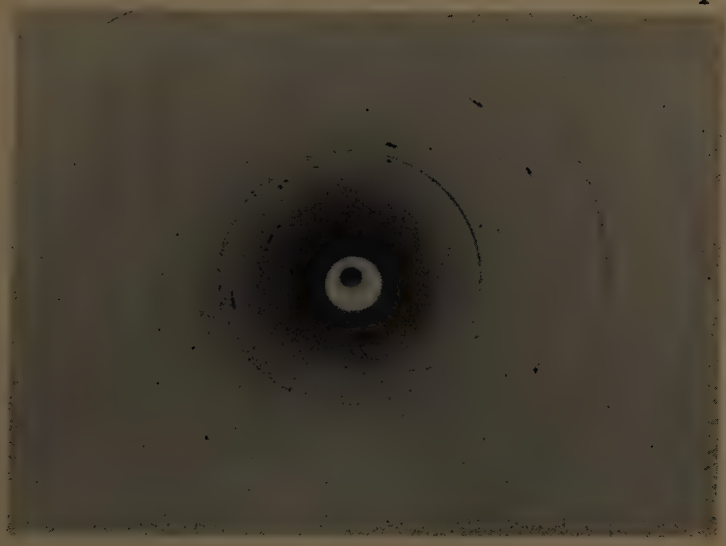

2

PLATE 3. X-ray texture of vein pitchblende, Wood Mine, Gilpin Co., Colorado, and massive pitchblende, Great Bear Lake, N. W. T., Canada.

have a density on the order of nine or greater, the amount of space between the fibers must be exceedingly small. The reduction from a theoretical density of approximately 11 can be accounted for by the density reduction due to oxidation. The fibers probably closely approach hexagonal symmetry in cross section since this allows the close packing necessary to maintain the observed density.

The upper diagram in PLATE 4 is from a fragment of a single crystal (0.3 cm. on edge) of uraninite from the Belgian Congo. The faint spots near the center of the picture are the Laue-spots resulting from the diffraction of the white radiation. The intense spot represents diffraction of the characteristic radiation by planes which chanced to be in the correct position to fulfill the requirements of the Bragg equation. The diffuseness of this reflection is the strongest evidence of the presence of a disordered structure in this sample.

The lower illustration of PLATE 4 was made using a spherule of UO_2 prepared by Leo Miller by precipitation from a uranyl ion solution with hydrogen sulphide at 15 atmospheres pressure and a temperature of 200° C. Some little spherules of UO_2 occured in a fine mass of brown microcrystalline UO_2. One of these spherules (0.03 mm. dia.) was mounted on a glass fiber with shellac, placed on a goniometer head, and mounted in a Buerger precession camera. This was done because the sample could be aligned by sighting through the collimator, which could then be placed in front of the X-ray source without disturbing the orientation of the sample. The picture itself was taken with the sample and film fixed in position, as in an ordinary Laue-diagram.

Under an optical microscope, the spherule appeared to consist of radiating needles. It was the purpose of this experiment to try to determine the crystallographic direction of the elongation axis of the needle-like crystals in the spherule by glancing the X-ray beam from the surface of the spherule. The spherule was so small in comparison with the area of the collimated beam that a glancing picture could not be obtained during the time that the precession camera was available for use. The diagram illustrated probably had most of the spherule in the beam, although the forward region diffraction takes place only from a thin rim of the spherule, as explained previously.

The diagram consists of faint Debye-Scherrer rings upon which are superimposed a large number of fine, sharply defined spots. The spherules evidently consist of radiating crystals larger than 10^{-3} cm. with interstices filled with much finer crystallites of random orientation. It will be noticed that all of the spots are doubled. The outer spots appear quadrupled. The outer spots have the two components of the alpha characteristic radiation resolved. The doubling that appears for all the spots is

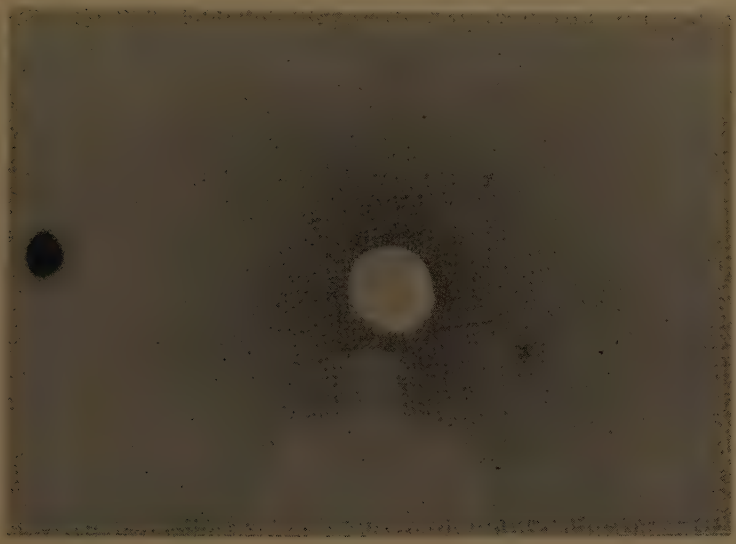

1

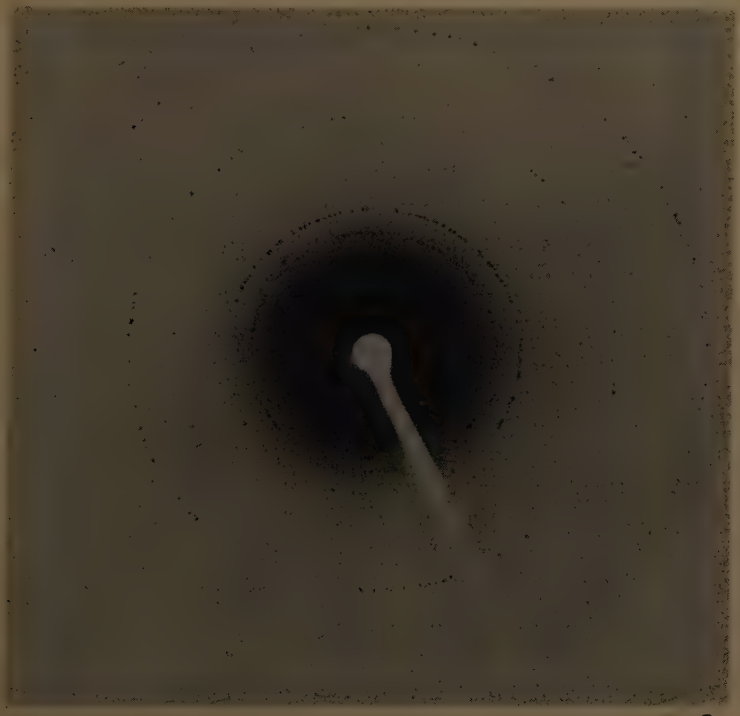

2

PLATE 4. X-ray texture of single crystal of uraninite, Belgian Congo; and synthetic UO_2.

due to the fact that double emulsion film was used with a very short specimen to film distance (3 cm.). The diffracted rays passed through the film at such an oblique angle as to blacken each emulsion at a position that made each spot resolved when viewed from directly above the surface of the film.

Conclusions. These experiments shed new information on the study of the crystal morphology of UO_2. It is reported (Palache, Berman, and Frondel, 1944) that the common crystallographic occurrences of uraninite are the octahedron, cubo-octahedron, and cube. Observation of uraninite specimens from many different localities in the mineralogical collections of Columbia University indicates that the most commonly occurring form is the cube. It is interesting that the zone of most dominant growth is the cube in pegmatites (where most uraninite specimens are found) whereas, in the vein type of deposit (pitchblendes usually), the octahedral plane is the plane of most rapid development. It is quite evident that the physicochemical conditions under which uraninite develops in a pegmatite and under which pitchblende develops in a vein are different. The crystal dimensions reflect this as well as the presence of large amounts of impurities in uraninite of pegmatitic origin and their absence in pitchblende.

Analysis of the Powder X-Ray Diffraction Data

Introduction. When monochromatic X rays are diffracted by a finely divided crystalline solid, certain maxima are produced. The position of these maxima is a function of the crystal geometry, the intensity a function of the atomic positions, and the profile of the maxima a function of the state of subdivision and lattice perfection of the sample. These effects will be briefly considered.

X-ray diffraction. When a beam of monochromatic X rays hits a single electron, a portion of the X rays are radiated in a spherical manner with the electron at the center of the sphere. The intensity of this coherently scattered radiation also has a spherical distribution. When the monochromatic beam hits an atom, the X-ray scattering intensity distribution is no longer spherical since it is due to the combined effect of the scattering from all of the extranuclear electrons. In this case, the scattering is strongest in the direction of the direct beam and drops off as the angle increases from the direct beam. This may be seen in the well-known "atomic scattering factor" curves (Hartree, 1925).

In the case of a crystal, which is a three-dimensional periodic distribution of scattering centers, there will be interaction between the waves scattered from each center. In certain directions, conditions will be such that reinforcement of the scattered X-ray waves will take place

and, in these directions, X-ray maxima can be detected. For an ideally imperfect crystal, the X-ray maximum will be a diffracted image of the X-ray source. The Debye-Scherrer method, in which the sample is a crystalline powder of completely random orientation, gives a series of diffraction images for any given reflection. These take the form of a cone with an apical angle of twice the Bragg angle. The intersection of a cylindrical film with the cones of diffracted rays produces the Debye-Scherrer arcs of the typical powder X-ray diagram.

In the modern type of Debye-Scherrer camera, a well crystallized solid, ground to a dimension of less than 10^{-3} cm. and randomly oriented, will produce very well defined diffraction maxima, provided the sample is of optimum thickness for its absorption coefficient. Under these conditions, the resolution and sharpness of the maxima depend directly upon the geometry of the camera.

Line broadening. Early in the history of X-ray diffraction, Scherrer observed that, as the size of individual crystallites or particles became less than 10^{-5} cm., the resolution and sharpness of the maxima became less for a given experimental geometry. This line broadening, even at that time, was related quantitatively to the size of the crystallites causing it. It should be noted that the line broadening is related to the crystallite dimension rather than to particle size only. One particle may be composed of several crystallites. These crystallites must have different orientations, since it is the difference in orientation that results in line broadening rather than any type of boundary effect.

Explanation. One may consider the physical explanation of diffraction-line broadening from two different viewpoints. One is the consideration of the crystal lattice as a three-dimensional diffraction grating and the treatment of it with the equations of optics. The other is the more elegant consideration of the reciprocal lattice.

In the first consideration, the repeating points of the crystal lattice may be considered analogous to the rulings of a diffraction grating. In the optical grating, the width of a spectral line depends upon the number of rulings on the grating. The greater the number of lines, the sharper will be any particular spectral line, thereby giving a greater resolution to any two adjacent lines. The same holds for diffraction by a crystallite. The greater the number of diffracting centers (atoms), the greater will be the diffraction resolution. This means that, as the crystallites become smaller, resolution is lost and the diffraction maxima become broader. This has been examined in a quantitative manner by Bragg (1933), who treats the diffraction effects by means of equations of optics and arrives at the same formula as Scherrer for line broadening in terms of crystallite

size. Bragg's derivation, which is quite simple, leads to a value of the constant in the equation which is very close to Scherrer's value.

In terms of reciprocal lattice theory, a real lattice set of planes is represented in reciprocal space by a point. When this point passes through the sphere of reflections, the primary X-ray beam is diffracted from the crystal to the reciprocal lattice point at the sphere of reflections. The diameter of the diffracted beam is theoretically the size of the point; that is, infinitely narrow. This assumes a primary beam of the same size. The point in reciprocal space represents a set of planes of infinite extent in real space. From the consideration of the construction of the reciprocal lattice, it may be shown that, as the planes in real space become smaller and more finite, the reciprocal lattice point representation begins to take on volume. As the extent of the real planes becomes very small, the reciprocal lattice point becomes a larger sphere (for simplicity, the reciprocal lattice point is considered spherical, but its true shape depends on the crystallite shape). This sphere, passing through the sphere of reflections, represents a diffraction far larger in size than the primary beam.

Limits of measurement. In modern types of cameras, line broadening may be observed when the crystallites are about 2000 Å. in size. The effect noticed is loss of resolution of the α_1 and α_2 components of the characteristic radiation in the high angle diffraction region. At about 1000 Å., the broadening is evident enough to permit precise measurements. By about 10^{-7} cm., the lines become so diffuse that precision of measurement becomes rather low.

Quantitative measure of crystallite size. In determining the quantitative relationships of crystallite size and some function of the diffraction maximum, the earliest measure was the "half-height breadth." This is the angular breadth of a diffraction peak measured at a height above the background level of one half of the height of the peak maximum. For parallel monochromatic radiation and a point specimen, Scherrer (1918) developed for crystallites of cubic form and isometric crystal system the following relationship:

$$\beta_x = \frac{C\lambda}{t \cos \theta}$$

where β_x = angular breadth of line (in radians),

t = edge dimension of cubic crystallite,

λ = wave length of X rays, and

θ = the Bragg angle.

When β_x is in radians and λ and t are in Angstrom units, von Laue, by rigorous analysis, shows C to equal 0.9. This is not his original value,

but one obtained by Jones (1938) after correcting certain mathematical errors in von Laue's paper. Jones has determined, by an independent method, the value of C to be 1.0, and he considers the value of t to be an apparent crystallite size.

The half-height breadth is not a really precise measure of the broadening of a diffraction line because of variability of the line profile. For example, some large crystallites will cause a sharpening of the upper part of the peak, while larger amounts of smaller crystallites will cause a broadening of the base. Von Laue has presented a concept of measurement that allows for greater precision. This is the idea of the "integral breadth."

If $I_{(x)}$ is the intensity at an angular distance x from the direction of maximum scattering and I_{max} is the maximum intensity of the line, the integral breadth is given by $\int I_{(x)}\, dx/I_{max}$. This means that, since the total area under the curve (the diffraction maximum) is proportional to the total X-ray scattering, the area divided by the maximum height of the curve gives a breadth which would represent a curve of the same energy but with a rectangular shape (a curve of uniform intensity). FIGURE 1 is a graphic representation of what this means. The limits of the integration are the points where the opposite tails of the maximum touch the base line, which represents the background scattering from the sample. The idea of integral breadth is valuable because it allows precise measurements to be made in spite of irregularities and assymmetrical maxima.

Disorder. Many types of disorder exist in crystalline materials. In general, these may be classed as strain or as fragmentation. Fragmentation disorder is found in cold-rolled metals where crystallites have been crushed and also, possibly, in metamict minerals. This gives the same geometrical effect as crystallite size line broadening. This type of broadening is proportional to $1/\cos\theta$, as can be seen from the equation of Scherrer.

In disorder caused by strain, crystal net-plane distances are not sharply defined. This type of disorder is proportional to $\tan\theta$. In metals, strain can be relieved by annealing. This is the basis of the heating experiments for studying metamict minerals. In ionic compounds, with which this work deals, the apparent strain disorder is really a distribution of unit cells of various dimensions caused by oxidation rather than direct stress. This will be demonstrated in a later part of this paper. Heating does not relieve this type of disorder.

Theory of experiments. Kochendörfer (1937) has demonstrated that one may treat a flat plate sample exposed to divergent radiation as a point specimen using the equation of Scherrer. This means that the trace

of a diffraction line profile obtained under conditions of Bragg focusing is equivalent to the line profile treated by Scherrer, Bragg, and von Laue, which was obtained by photometering a Debye-Scherrer film.

Kochendörfer treats of a general unsymmetrical case where the flat sample is not coincident with the center of the X-ray beam. The limiting case of this, the symmetrical sample (as in the "diffractometer" manufactured by Norelco), leads to the same expression von Laue obtained for the point specimen. This shows that the Bragg focusing will give the same integral breadth as in the ideal case.

The diffractometer. The Norelco diffractometer used in these meas-

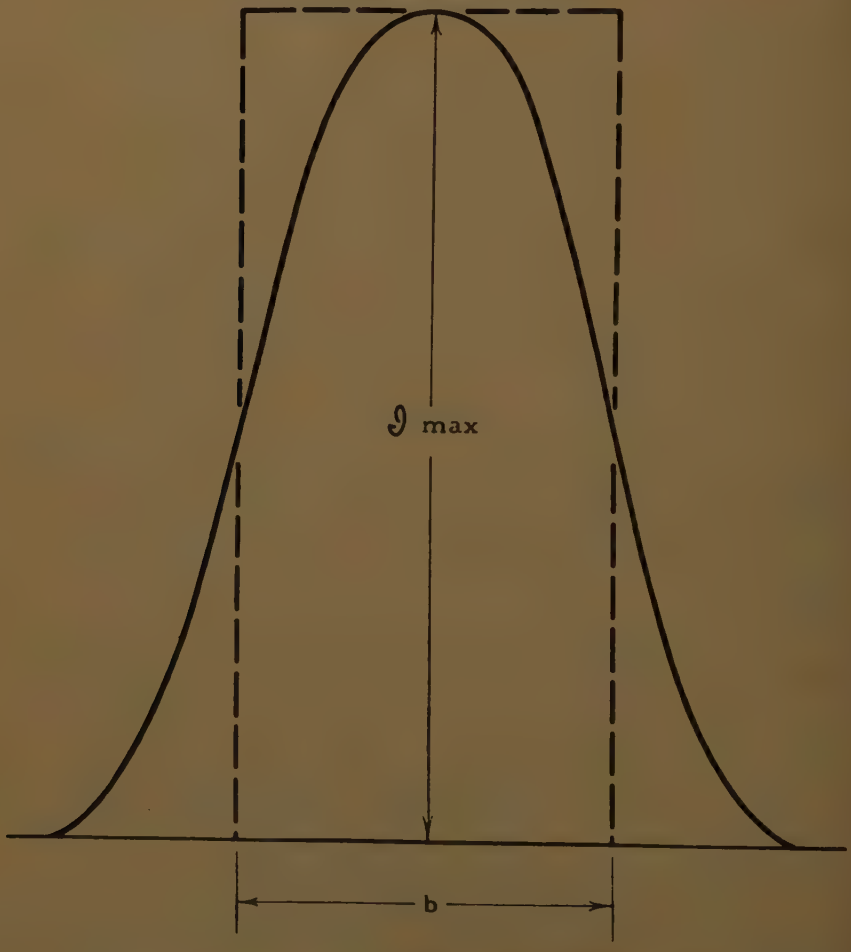

FIGURE 1. Diagram to illustrate the idea of integral breadth.

urements is the equivalent of a semifocusing type of powder X-ray diffraction camera in which the diffraction record is made by a Geiger counter traversing the focusing circle of the camera and recording diffraction intensity as a function of Bragg angle by means of suitable scaling circuits and recorder. The diffractometer acts as an asymmetrical focusing camera in which the radius of the focusing circle is a function of the angle of the specimen plane with the main beam. The specimen surface is a plane 20 mm. × 10 mm. The "focusing circle" lies in a plane normal to the horizontal central axis of the diffractometer at the mid-point of the specimen and is defined by the long axis of the X-ray tube focal spot, the axis of the diffractometer and the receiving slit in front of the Geiger tube. The diameter of the focusing circle varies between infinity at 0° (2 θ) and approximately 17 cm. at 180° (2 θ).

The advantage of the diffractometer over film methods is that line profiles are obtained by direct diffraction without the necessity of having to photometer a film and to correct for sensitivity of the emulsion. It is necessary, of course, that the diffractometer be adjusted so that it records the intensity in a linear manner at the correct angular values. The detecting and recording device used in the diffractometer is a Geiger-Muller counter connected to suitable electronic scaling circuits that convert the X-ray intensity to a chart record which is a plot of the linear value of intensity against the Bragg angle. Since the measurements of integral intensity are made directly from the chart, it is important for the diffraction peaks to be recorded entirely within the linear range of the recording apparatus. The linearity is determined by putting a strong X-ray signal into the counter and then reducing this signal by integral amounts with absorbers of known thickness. By properly plotting the values obtained by measuring the signal through different absorber thickness, the linear region can be determined. The absorption of X rays follows the relationship:

$$I = I_o e^{-\mu t}$$

where I = measured intensity,
I_o = incident intensity,
μ = linear absorption coefficient, and
t = thickness.

Taking the logarithm of both sides of the expression, it may be seen that for a constant I_o, as can be set up in this experiment, t will vary in a linear manner with the log of I. This may easily be plotted and the deviation from linearity observed directly from the plot. FIGURE 2 shows the linearity plot of the Geiger tube that was used during the course of the measurements described in this paper. The tube was operated at a po-

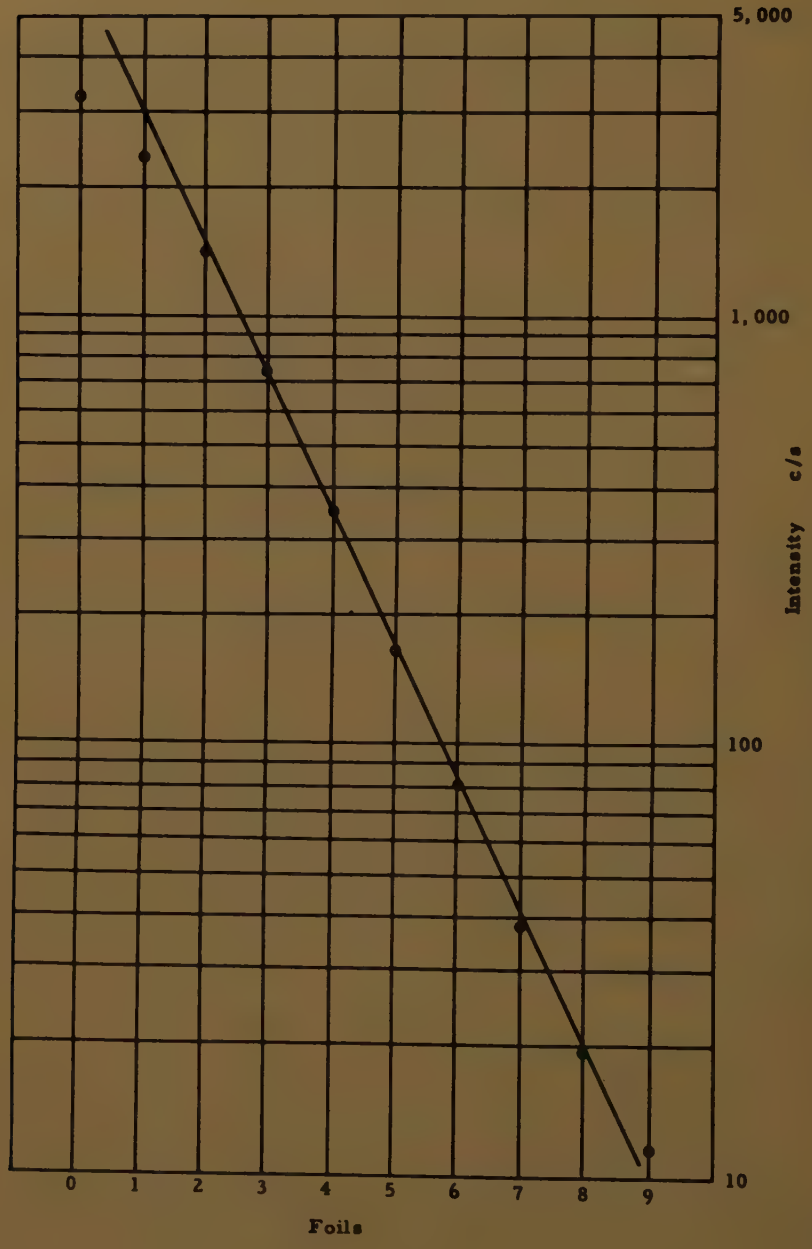

FIGURE 2. Linearity curve for Geiger tube.

TABLE 1

LINEARITY OF GEIGER TUBE

Foils	Total count	Time (sec.)	C/S
0	25,684	8.0	3210
1	25,635	10.8	2373
2	25,619	18.2	1407
3	25,611	33.8	758
4	25,611	70.8	361
5	25,604	152.2	168
6	25,601	324.8	79
7	12,801	335.0	38
8	3,200	162.4	19.7
9	1,600	137.0	11.7
10	800	105.0	7.6
11	200	38.0	5.2

These values were determined using nickel foils 0.0007 inches in thickness.

tential of 1,600 volts. This value was selected by determining experimentally the plateau of the tube. The data obtained in the linearity test are given in TABLE 1.

Flat specimen error. The instrument is designed for flat specimens 10 × 20 mm. The use of a flat rather than a curved specimen, whose radius of curvature must continuously vary with the Bragg angle, produces no significant errors. The magnitude of the flat specimen error is expressed by

$$\Delta\theta = \frac{\sin 2\theta}{1.6\mu}$$

where μ is the linear absorption coefficient.

For a material such as quartz, the flat specimen error for the 100 reflection ($\theta = 10.438°$) is only 0.0022°. The absorption coefficient of quartz is only 90.3, whereas the coefficient for UO_2 is on the order of 3,000, so that this error is very insignificant.

Angular adjustment. The angular adjustment of the diffractometer was checked and adjusted on the basis of a silicon plate whose lattice parameter was determined to be such that the 400 reflection is 60.130° (2 θ). This was determined by Doctor William Parrish using focusing techniques and film cameras. The diffractometer was checked regularly during the course of the measurements and at no time did the calibration vary more than 0.02°. This was easily adjustable.

Correction for nonhomogenous radiation. The equations relating integral breadth to crystallite size or disorder presuppose the use of monochromatic radiation in the experimental measurements. The $k\alpha$ component of the copper characteristic radiation used in these measure-

ments is really a doublet composed of the wave lengths $k\alpha_1$ and $k\alpha_2$, consequently all of the observed diffraction maxima will be broadened by this effect. At high Bragg angles these two different wave lengths are resolved so that they may be directly observed. This may be seen in the upper curve of FIGURE 2, which is a tracing of actual recorded data.

Brill (1928) has approximated the diffraction line shape as overlapping triangles and developed an expression for determining the true breadth of the α_1 component.

Jones (1938), by more closely approximating the diffraction line shape mathematically, develops a graphical expression which may be used to correct the overlapping components for the extra breadth due to α_2. This is illustrated in FIGURE 3. The meaning of the ratios is as follows:

$$\frac{B}{B_o} = \frac{\text{true breadth}}{\text{observed breadth}}$$

$$\frac{d}{B_o} = \frac{\text{doublet separation}}{\text{observed breadth}}$$

The doublet separation has been calculated and plotted in FIGURE 4. The curve gives the angular separation for copper k radiation in terms of Bragg angle. The numerical values from which this curve is constructed

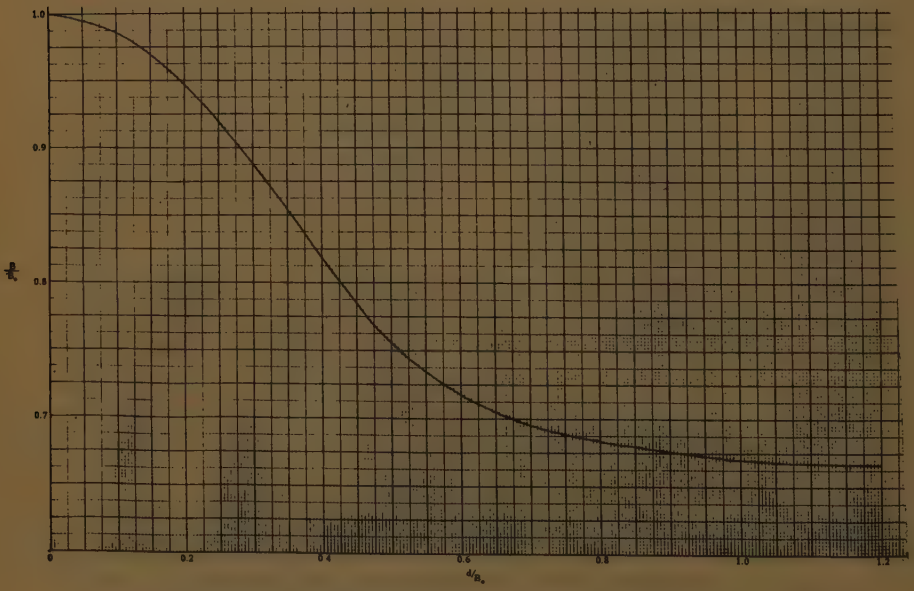

FIGURE 3. Jones's curve for correcting for α_2 breadth.

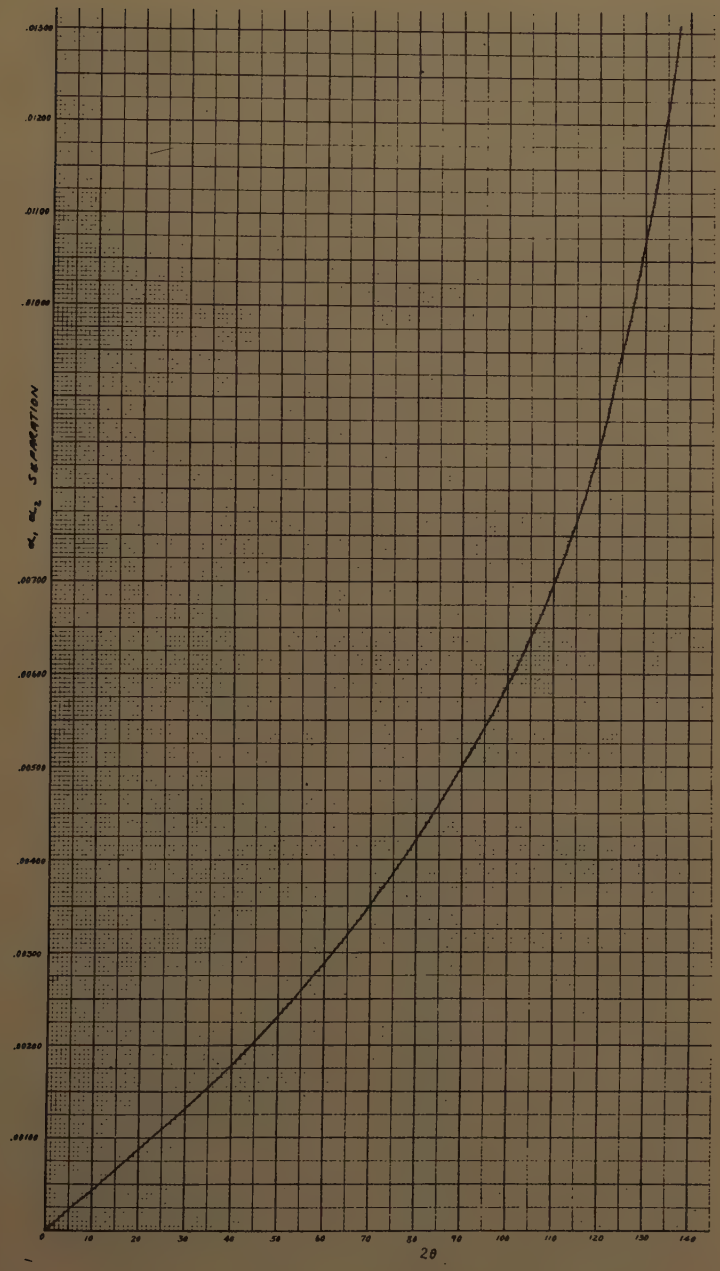

FIGURE 4. Angular separation of α_1 and α_2 for different Bragg angles.

are listed in TABLE 2. The values of the separation were computed from the Bragg equation by using given values of the interplanar spacing and computing the Bragg angle for each of the two component wave lengths. From these, the differences were obtained.

Measurement of broadening. Powder consisting of particles of "infinite size" (greater than 10^{-4} cm.) will always give lines of finite breadth, much greater than the true diffraction breadth. The observed breadth of the lines given by such particles depends on the geometry of the apparatus used. Scherrer considered that the true diffraction breadth could be obtained by taking the linear difference of the measured breadth and an instrumental constant. This constant is determined from consideration of the instrument geometry. He assumed this constant to be independent of 2θ. Scherrer's results on measurements of gold colloids were in good agreement with results obtained by independent methods. Jones's approach to the problem is to mix with his unknown sample a powder of crystallite size large enough to be considered infinite. Of course, the lines from the two different materials must not overlap. He obtains on film so-called "sharp lines" which represent only the instrument factors. Jones considers the shapes of the line profiles, and he develops correction curves for determining the true broadening but, in general, his curves do not vary greatly from the linear relation-

TABLE 2

ANGULAR SEPARATION OF THE NONHOMOGENOUS COMPONENTS OF COPPER CHARACTERISTIC RADIATION

hkl	2θ	Separation (radians)
111	28.25	0.00124
220	46.97	0.00216
311	55.71	0.00264
222	58.43	0.00276
400	68.61	0.00340
331	75.79	0.00388
420	78.15	0.00406
422	87.32	0.00476
333-511	94.18	0.00536
440	105.72	0.00658
531	112.98	0.00754
600-442	115.48	0.00792
620	126.12	0.00986
533	135.13	0.01216
622	138.45	0.01264

Wave-length values used were as follows: λ k α_1 1.54050 Å.
k α_2 1.54434 Å.
Data are computed for a cubic face centered structure (CaF_2).

ship of Scherrer. Inspection of FIGURES 5a and b, showing the variety of line profiles observed in this study, will show that a more approximate method would be useful, especially if it could take advantage of the fine resolution and stability of the diffractometer.

The modern diffractometer is stable and gives data of sufficient reproducibility to permit sharp line material to be examined independently of the unknown material. It was observed that the breadth of a sharp line material is not uniform over the entire angular range, therefore not independent of 2 θ. In this work, the measured and corrected breadths of the sharp line material were plotted against the Bragg angle and interpolated to points where they could be linearly subtracted from the observed broadened lines. The sharp lines are corrected for α_2 broadening, and so are the broadened lines. This is done before subtraction.

During the early part of this work, it was proposed to use the mineral fluorite (CaF_2), which is structurally the same as UO_2 as a sharp line material. When the corrected integral breadths of fluorite were plotted, however, they showed an extremely erratic distribution. It was then realized that the diffracting power of this material was such that the intensity of many of the maxima went far beyond the linear range of the Geiger tube. In addition, the extremely well-developed cleavage of fluorite causes a preferred orientation which strongly affects the peak heights. In order to eliminate these effects, quartz (SiO_2) was used with much better results. This mineral was selected because a large strain-free crystal could be obtained and, furthermore, it does not have any cleavage. A crystal was crushed and ground so that the fragments were less than 400 mesh. This gave crystallites of essentially infinite dimension. The fact that some broadening is produced by small particles resulting from the grinding process does not affect the final results, since the unknown samples are subject to the same grinding process as the sharp line producing material.

The lower curves on FIGURE 6 show the integral breadth (corrected for α_2 broadening) for quartz used as a standard for the determination of instrumental breadth. The curve is in two sections, since a different slit system is used for the low-angle region on the diffractometer than is used for the high-angle region. The reason for this is that as the Geiger tube traverses the focusing circle, the sample also rotates and, at higher angles, a given X-ray beam divergence covers a smaller part of the sample than at lower angles. For this reason, at higher angles larger slits may be used. As may be seen from Kochendörfer (1937), this changing of slits does not affect the line broadening due to the crystallite size and disorder.

As an example of the real significance of the measurements, the

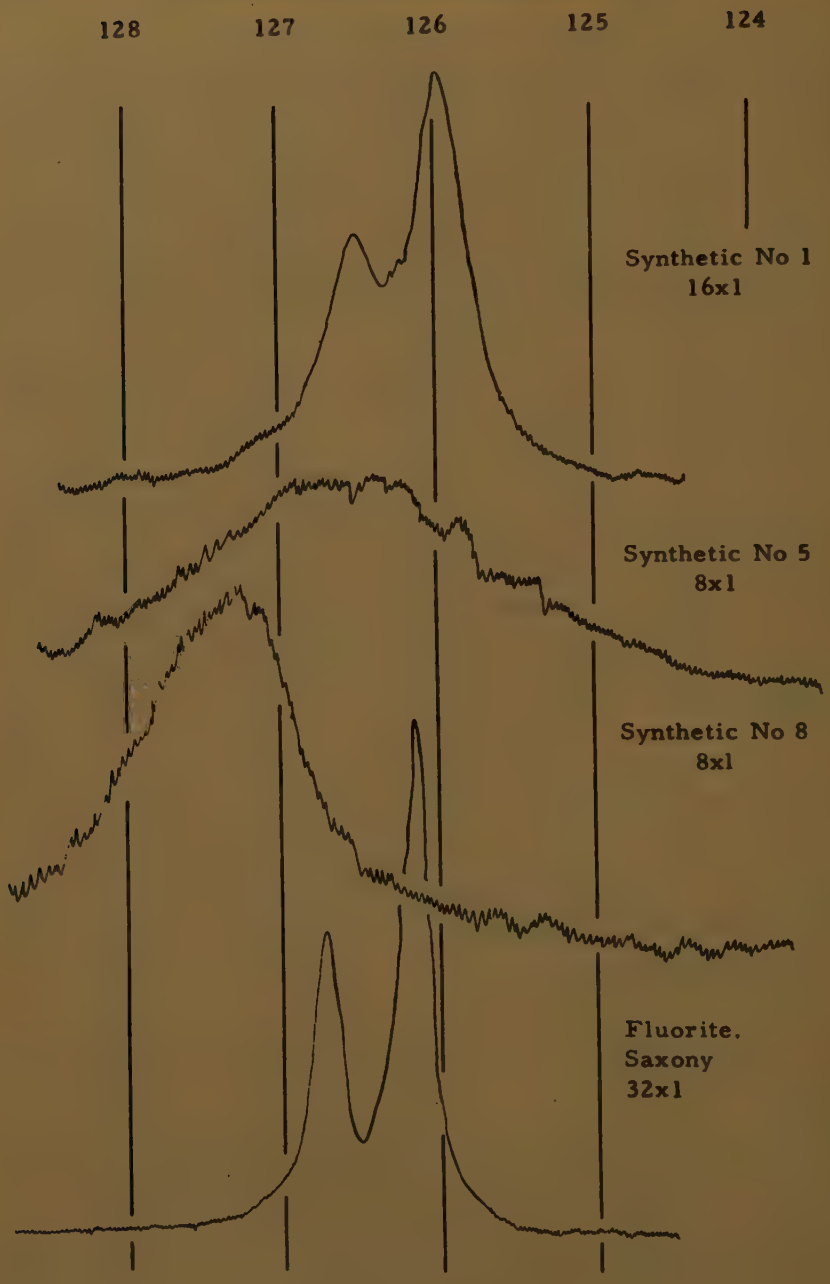

FIGURE 5a. Diffractometer curves for synthetic samples.

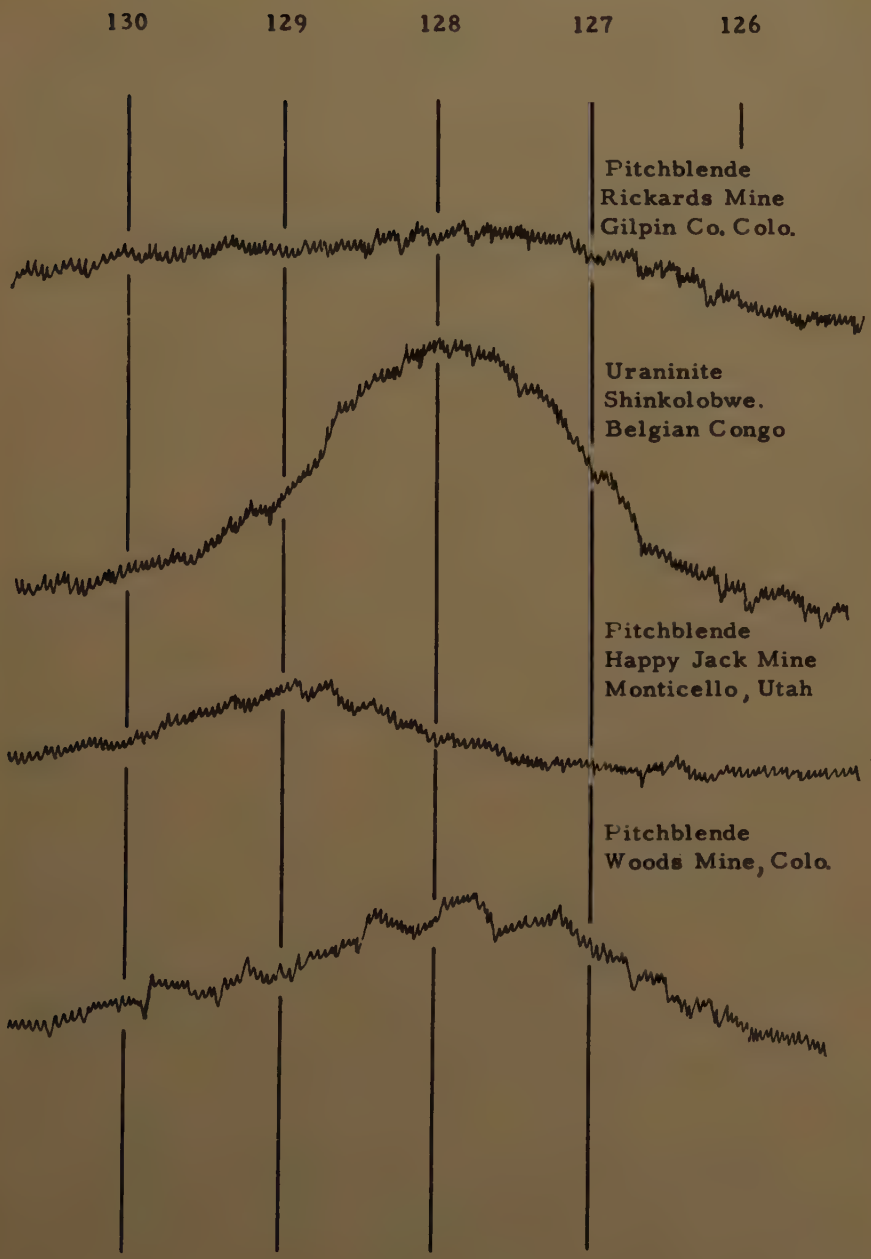

FIGURE 5b. Diffractometer curves for natural samples.

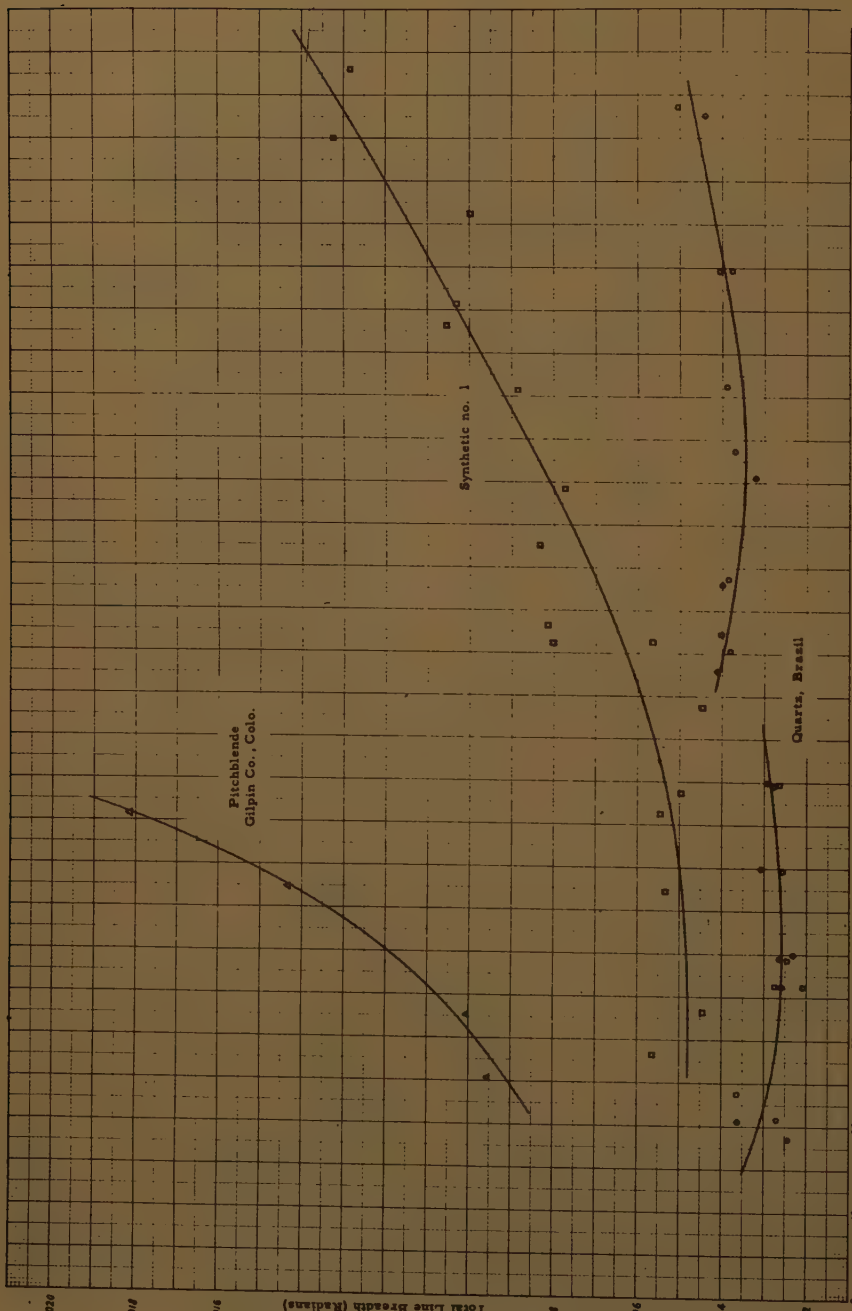

FIGURE 6. Integral breadth of quarts versus Bragg angle.

total corrected line breadths of two other samples are plotted on the same sheet. One is a synthetic sample of fairly large crystallite size and small disorder parameter, and the other, a highly disordered pitchblende.

Preparation of samples. In order to prevent superposition of diffraction lines of accessory minerals over the diffraction lines of the UO_2 samples, the specimens had to be prepared as carefully as possible. The various methods of mechanical purification have been tried, such as the Frantz isodynamic separator, heavy liquids, and panning. The best way to obtain a pure sample is to crush the material to about 50 mesh and to pick out the homogenous appearing grains under a binocular microscope. This method has been found to give the smallest amount of extraneous X-ray diffraction peaks. Because of the selective rather than the random nature of this study, it has been possible to reject samples which contain intimately intergrown impurities. For the X-ray diffraction examination, the samples are crushed to pass a 100 mesh screen and then ground in an agate mortar to less than 400 mesh.

Measurements and calculations. The chart recorder of the diffractometer was run so that one inch of chart paper is equal to one degree 2θ. The base line of the peaks is constructed by extending the base line from the zones between the peaks. The maximum height of the peak is measured with a scale to the nearest 0.01 inch. The area is then measured with a polar planimeter to the nearest 0.01 square inch. An average of three readings is used. In Appendix A, examples are presented of measurements made on various samples. The maximum height column is labeled I_{max}, the area under the curve is labeled I_{tot}. The observed integral breadth obtained by dividing I_{tot} by I_{max} is in the column B_{raw}. This value is given in degrees 2θ. This is converted to radians in the column $B_{\substack{rad \\ raw}}$. It is used with Jones's chart (FIGURE 3) for correcting the broadening due to the α_2 component of the characteristic radiation. In order to use that chart, the angular separation of the α_1 and α_2 components for the Bragg angle of the peak is obtained from FIGURE 4. The value of the real broadening b is obtained by taking the linear difference of $B_{\substack{rad \\ corr}}$ and the value of the pure instrumental broadening at the same Bragg angle. This pure instrumental broadening is obtained from the curve plotted for quartz (FIGURE 6). The next few columns are self-explanatory. The $b \cos \theta$ and $b/\tan \theta$ values are used to determine the cause of the line broadening. In the later columns, some values of d, the interplanar spacing, have been calculated, and from these the unit cell dimension. The column labeled t is the crystallite dimension based on Scherrer's formula, given in Ångstrom units.

Line-broadening results. The plots of $b \cos \theta$ and $b/\tan \theta$ are shown in FIGURES 7 and 8 for some of the samples examined. Three synthetic samples of UO_2 were studied. These samples, prepared by Leo Miller, represent materials grown under different conditions. The sample labeled Experiment No. 1 was precipitated from a uranyl ion solution containing ferrous ions with hydrogen sulfide at approximately 200° C. and 15 atmospheres pressure. Some tiny spherules which occurred in this precipitate were examined in the first portion of this paper. The entire precipitate was ground and examined by an X-ray diffractometer. The interplanar spacing and the lattice dimensions obtained from each spacing are presented in TABLE 3. These values are an excellent illustration of the precise measurements that can be made with the diffractometer, using ordinary care in sample preparation and normal operating procedure.

Examination of the curve for $b \cos \theta$ shows an almost horizontal array of points. This indicates a very close following of the cosine relationship as expressed by the formula of Scherrer. It is very indicative of the absence of disorder. The $b/\tan \theta$ has a slight negative slope. This curve is plotted with a vertical scale two and one-half times smaller than the cosine curve, so that it is consistent with the rest of the curves in this paper. If the tangent curve in this case were plotted on the same scale as the cosine curve, it would have a much greater slope.

A second synthetic sample (Experiment No. 5) was produced under conditions similar to the first, except that the temperature was lower 135° C.). In this case, the diffraction lines are much broader. The formula of Scherrer gives, in this case, a crystallite dimension of only 1/5 that of the first experiment. Examination of the cos and tan curves for this sample shows that the cos curve is still horizontal, although the points are very much more widely scattered, and the $b/\tan \theta$ curve has a much greater slope. These are the expected effects for a reduced crystallite dimension. The crystallite dimensions for the synthetics are listed in TABLE 4. One explanation for the greater spread of points on this curve is that perhaps some shape function of the crystallites is involved.

In both the first and second samples, the greatest crystallite dimension appears to be in the direction perpendicular to the 001 planes. The larger crystallites of the first sample are known to be elongated, but it was not possible to tell the crystallographic direction of elongation. The elongation in the case of these synthetics is apparently not in the same crystallographic direction as the elongation observed in some natural pitchblendes in the first part of this paper. The lattice parameters of this sample appear to be essentially the same as those of the first

FIGURE 7. Cos and tan curves for synthetic UO_2.

FIGURE 8. Cos and tan curves for natural UO_2.

TABLE 3

SAMPLE: SYNTHETIC NO. 1

hkl	d	a_o
111	3.1552	5.465
200	2.7329	5.466
220	1.9327	5.466
311	1.6483	5.467
222	1.5778	5.465
400	1.3668	5.467
331	1.2542	5.467
420	1.2224	5.467
422	1.1159	5.467
511-333	1.0523	5.468
440	.96649	5.467
531	.92422	5.468
600-442	.91125	5.468
620	.86447	5.468
533	.83377	5.467
622	.82428	5.467

one, although the precision of the determination is lower due to the diffuse maxima in the second sample.

Electron micrographs of these two samples show the presence of lathlike "crystals" of UO_2. The general appearance of the first and second sample is the same, although the second sample contains definitely smaller laths. The magnifications are not reliable, but some of the laths in the first sample have widths that appear to be of the order of 1000 Å., and some of the laths in the second sample on the order of

TABLE 4

CRYSTALLITE DIMENSIONS OF SOME SYNTHETIC UO_2 SAMPLES

hkl	Dimensions (Å.)		
	Exp. 1	Exp. 5	Exp. 8
111	532	109	516
200	898	140	595
220	608	113	410
311	632	121	382
222	798	168	
400	1290		
331	725	82 (113)	
420	454	117 (91)	
422	442	102	
333-511	545	97	
440	483	143	
531	406		
600-442	438		
620	566	101	
533	438		
622	498		

500 Å. In the first sample, some spherules occurred on the order of 0.003 cm. diameter. In electron micrographs of the second sample, some spherules were observed on the order of 0.00005 cm. diameter.

There is no evidence that the laths in the electron micrographs are single crystallites, or even that they are representative of the sample as a whole. Very often, such pictures represent the subjective impulse of the operator to photograph something striking or unusual. The X-ray line broadening determination represents an average picture of the scattering by an entire sample.

A third synthetic sample (Experiment No. 8) was produced under conditions similar to those of the first, except that some air was present in the system. The lattice parameter of this sample shows an immediate decrease from 5.468 for Experiment No. 1 to 5.44. This indicates a structure with an oxygen content higher than $UO_{2.0}$. It is probably close to $UO_{2.3}$ (Katz and Rabinowitch, 1951). The cosine curve shows a definite positive slope, and the tangent curve is nearly horizontal, which indicates that line broadening very definitely follows a disorder expression. The crystallite size is probably as large as in the first sample, which explains why it is so completely overshadowed by the disorder effect.

A single crystal (0.2 cm. across) of uraninite from the Belgian Congo was ground, X-rayed, and the line broadening measured. This should be material of infinite crystallite dimension. The horizontal slope of the $b/\tan\theta$ curve shows that there is no crystallite size component in the line-broadening function. This same sample is examined in a later section, where it is shown that the line broadening is a function of the distribution of different size unit cells.

This uraninite and all of the pitchblendes examined have lattice parameters less than the theoretical 5.460 for $UO_{2.0}$. A completely stoichiometric UO_2 is almost never found in nature. Three pitchblende samples whose data is presented here all show a definite positive slope to the curve for the function $b \cos\theta$, indicating the excess oxygen in each.

The least oxidized sample appears to be the pitchblende from the Happy Jack Mine, Monticello, Utah. It has an apparent crystallite dimension on the order of 300 Å. Some other crystallite dimensions are listed in TABLE 5.

The slope of the $b/\tan\theta$ curve may be either positive or negative. A possible explanation for this is that, if there is strong crystallite size broadening, the curve will be positive, but if the crystallite size broadening is small, the slope may be negative.

Line-broadening conclusions. This method, although not original,

TABLE 5

CRYSTALLITE DIMENSIONS OF SOME PITCHBLENDE SAMPLES

	hkl	t
Happy Jack Mine	111	300 Å.
Monticello, Utah	200	319
	220	217
	311	221
	222	340
Rickards Mine,	200	215
Gilpin Co., Colo.	220	143
	311	112
Hummelfurst, Saxony,	111	168
East Germany	200	171
	220	128
	311	103

never seems to have been used to examine ionic compounds. It appears to be sensitive enough to show when disorder and when crystallite size line broadening are in the powder diffraction pattern of a material. It gives a good idea of the reliability of a crystallite size determination based on the formula of Scherrer. It also shows that, in these cases, X-ray diffraction powder diagrams from pitchblende show line broadening to a large degree because of disorder rather than because of small crystallite dimensions.

Line Broadening Due to Variation in Lattice Parameters

It is known that oxidation of UO_2 changes the dimensions of the unit cell (Katz and Rabinowitch, 1951). This effect apparently takes place in a linear manner. In this work, broadening of Debye-Scherrer maxima have been observed. It is thought that this broadening is a function of the variation in lattice dimensions within a given sample. In other words, the shape of any one broadened maxima not having crystallite size broadening may be considered to represent a function which gives the distribution of lattice parameters. This follows from Bragg's law and from the assumption that the intensity at any point on the curve is proportional to the fraction of unit cells in the sample having the dimension fitting the Bragg angle at that point. This, of course, is for cubic substances only. From Bragg's law and the index relationship for the isometric system, with which we are concerned here, it is possible to obtain an expression for the distribution of the integral breadths in a diffraction pattern.

The curve (FIGURE 9) represents a diffraction maxima for an isometric substance as observed on the X-ray diffractometer. On the

diagram, the line 1, 2 represents the integral breadth. The value of this is the angular difference between θ_2 and θ_1. The angle θ represents the most abundant unit cell dimension in the sample. This dimension is a_o. The cell dimensions represented by the angles θ_1 and θ_2 are a_1 and a_2. Let $a_1 - a_2 = \Delta a$. In any given sample, $\frac{\Delta a}{a_o}$ will be a constant. The integral breadth, $\theta_2 - \theta_1$ is called $\Delta\theta$. We are interested in determining the change of $\Delta\theta$ with respect to θ in terms of the lattice parameter, the indices of the line and the Bragg angle.

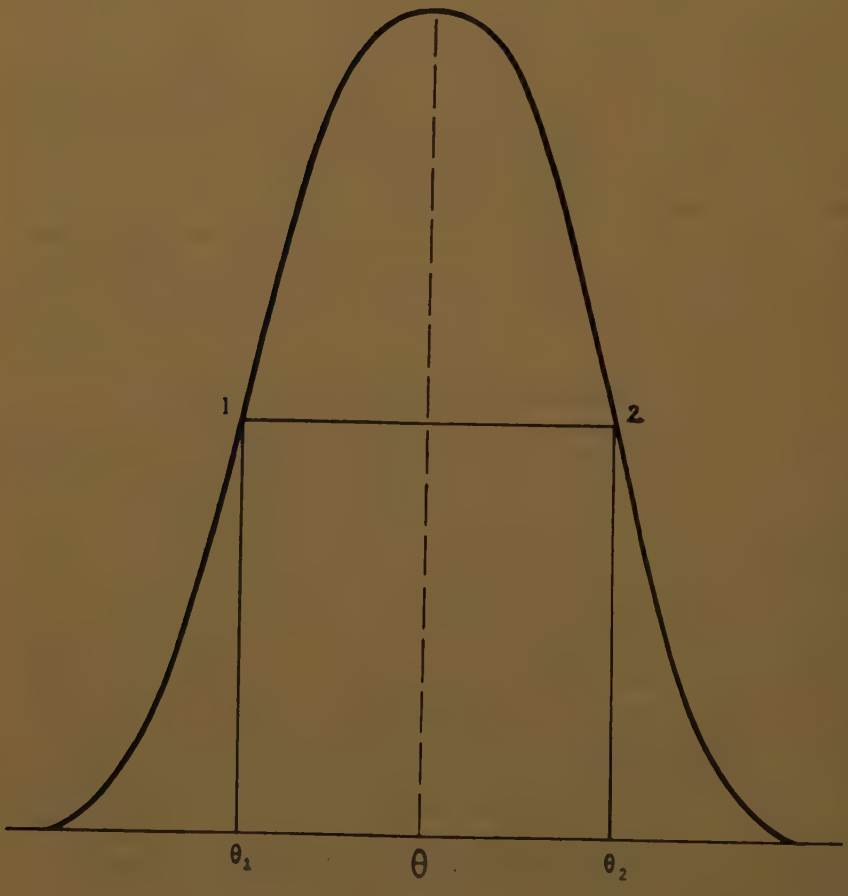

FIGURE 9. Diagram to illustrate disorder parameter.

We know the Bragg relationship:

(1) $$n\lambda = 2d \sin \theta.$$

From the geometry of the isometric system we know that

(2) $$d = \frac{a_o}{\sqrt{h^2 + k^2 + l^2}}$$

This leads us to

(3) $$n\lambda = \frac{2a_o \sin \theta}{\sqrt{h^2 + k^2 + l^2}}$$

and

(4) $$a_o = \frac{n\lambda\sqrt{h^2 + k^2 + l^2}}{2 \sin \theta}$$

From the diagram (FIGURE 9) and the last equation we see that

$$a_2 = \frac{n\lambda\sqrt{h^2 + k^2 + l^2}}{2 \sin \theta_2}$$

and

$$a_1 = \frac{n\lambda\sqrt{h^2 + k^2 + l^2}}{2 \sin \theta_1}$$

Combining the last two equations, we get

$$\Delta a = \text{constant} = a_1 - a_2 = \left(\frac{n\lambda\sqrt{h^2 + k^2 + l^2}}{2}\right)\left(\frac{1}{\sin \theta_1} - \frac{1}{\sin \theta_2}\right)$$

Let

$$\frac{n\lambda\sqrt{h^2 + k^2 + l^2}}{2} = K.$$

We get

(5) $$\Delta a = K\left(\frac{1}{\sin \theta_1} - \frac{1}{\sin \theta_2}\right)$$

By previous definition

(6) $$\Delta \theta = \theta_2 - \theta_1 .$$

Since θ is the mean of θ_2 and θ_1 (this is on the assumption of a symmetrical distribution curve).

(7) $$\theta = \frac{\theta_1 + \theta_2}{2}$$

From (6) we see

(8) $$\theta_2 = \Delta\theta + \theta_1$$

and

(9) $$\theta = \frac{\theta_1 + \Delta\theta + \theta_1}{2} = \theta_1 + \frac{\Delta\theta}{2}$$

so that

(10) $$\theta_1 = \theta - \frac{\Delta\theta}{2}$$

From (8)

(11) $$\theta_1 = \theta_2 - \Delta\theta$$

from (7)

(12) $$\theta = \frac{\theta_2 - \Delta\theta + \theta_2}{2} = \theta_2 - \frac{\Delta\theta}{2}$$

We get

(13) $$\theta_2 = \theta + \frac{\Delta\theta}{2}$$

Substituting EQUATIONS Nos. 10 and 13 in No. 5

$$\Delta a = K\left(\frac{1}{\sin(\theta - \frac{\Delta\theta}{2})} - \frac{1}{\sin(\theta + \frac{\Delta\theta}{2})}\right)$$

Let $$\theta = a$$

Then $$\frac{\Delta\theta}{2} = b$$

$$\Delta a = K\left(\frac{1}{\sin(a-b)} - \frac{1}{\sin(a+b)}\right)$$

$$\Delta a = K\left[\frac{\sin(a+b) - \sin(a-b)}{\sin(a-b)\ \sin(a+b)}\right]$$

$$= K\left[\frac{\sin a\cos b + \cos a\sin b - \sin a\cos b + \sin b\cos a}{\sin^2 a - \sin^2 b}\right]$$

(14) $$\Delta a = K\left(\frac{2\cos a\sin b}{\sin^2 a - \sin^2 b}\right)$$

Replacing the assumed letters by their true values, we get

$$\Delta a = \left(\frac{n\lambda\sqrt{h^2+k^2+l^2}}{2}\right)\left(\frac{2\cos\theta\sin\frac{\Delta\theta}{2}}{\sin^2\theta-\sin^2\frac{\Delta\theta}{2}}\right)$$

Since

$$\sqrt{h^2+k^2+l^2} = \frac{2a_o\sin\theta}{n\lambda} \quad \text{from (4),}$$

we get

$$\Delta a = a\sin\theta\left(\frac{2\cos\theta\sin\frac{\Delta\theta}{2}}{\sin^2\theta-\sin^2\frac{\Delta\theta}{2}}\right)$$

$$\frac{\Delta a}{a_o} = \sin\theta\left(\frac{2\cos\theta\sin\frac{\Delta\theta}{2}}{\sin^2\theta-\sin^2\frac{\Delta\theta}{2}}\right)$$

$$(15) \qquad \frac{\Delta a}{a_o} = \frac{\sin 2\theta\sin\frac{\Delta\theta}{2}}{\sin^2\theta-\sin^2\frac{\Delta\theta}{2}}$$

Since we are interested in the value of $\Delta\theta$ in terms of the angle θ, we must arrive at the solution in terms of the quadratic formula:

$$ax^2 + bx + c = 0$$

$$x = \frac{-b \pm \sqrt{b^2-4ac}}{2a}$$

From EQUATION No. 15

$$\left(\frac{\Delta a}{a_o}\right)\left(\sin^2\theta\right) - \left(\frac{\Delta a}{a_o}\right)\left(\sin^2\frac{\Delta\theta}{2}\right) - \sin 2\theta\sin\frac{\Delta\theta}{2} = 0.$$

Let $\sin\frac{\Delta\theta}{2}$ be the unknown.

$$(16) \quad -\left(\frac{\Delta a}{a_o}\right)\left(\sin^2\frac{\Delta\theta}{2}\right) - 2(\sin\theta\cos\theta)\left(\sin\frac{\Delta\theta}{2}\right) + \left(\frac{\Delta a}{a_o}\right)\left(\sin^2\theta\right) = 0.$$

This can now be substituted into the quadratic formula

$$\sin\frac{\Delta\theta}{2} = \frac{2\sin\theta\cos\theta \pm \sqrt{4\sin^2\theta\cos^2\theta + (4)\left(\frac{\Delta a}{a_o}\right)^2 \sin^2\theta}}{-2\frac{\Delta a}{a_o}}$$

This may be simplified to

$$\sin\frac{\Delta\theta}{2} = \frac{\sin\theta\cos\theta \pm \sin\theta\sqrt{\cos^2\theta + \left(\frac{\Delta a}{a_o}\right)^2}}{-\frac{\Delta a}{a_o}}$$

Starting with an integral breadth obtained from a 001, reflection $\frac{\Delta a}{a_o}$ may be calculated. Using this value, one may calculate the integral breadths of all other reflections if the broadening is due solely to a distribution of different lattice parameters. It will be noticed that the positive value of the numerator of the expression gives a result of no meaning, since the fraction will have an absolute value greater than unity. This is not possible for the sine function. Since the sine term of the resultant is for a very small angle, it is quite sensitive to small deviations. It was found necessary to maintain at least the sixth decimal place in order to have meaningful results.

On the basis of the derived equation, values are plotted for the line breadth of a uraninite (single crystal, Belgian Congo) sample (FIGURE 10). The value of $\frac{\Delta a}{a_o}$ is determined from the 002 reflection of the measured sample. This value is used to compute the theoretical broadening of the other possible X-ray reflections. These (circles) are plotted against the Bragg angle. The measured values (triangles) are plotted on the same sheet. The agreement seems to be good except for the small difference in slope angle of the two curves. This indicates a possible systematic difference. Two factors may be the cause of this. One is the assumption that the distribution of varying lattice parameters is a symmetrical function. This seems like a valid assumption on the basis of the observed symmetry of the measured X-ray reflections. A method of plotting using a higher order reflection for the source of the value of $\frac{\Delta a}{a_o}$ would have given even better agreement of the two curves. A small change of $\Delta\, 2\,\theta$ at small Bragg angles will cause a rather larger change at higher angles, whereas a change at higher Bragg angles will cause only a small change at smaller angles.

An alternative method of plotting the theoretical curve consists of taking a $\frac{\Delta a}{a}$ value from one reflection and computing values of da_1 and

da_2 for each reflection. From these, values ot θ_1 and θ_2 can be calculated and the differences determined for each reflection (see Appendix B). These can be plotted against the Bragg angle and give essentially the same result as the derived expression. This alternative method is cumbersome, but may be used as a check on the trigonometric computations (it should be noted that the diffraction curve is not a true distribution function because of the addition of instrumental line broadening effects).

U_3O_8. Above 250° C., uraninite, which contains more oxygen than $UO_{2.0}$, will form the compound U_3O_8 even in an inert atmosphere. With longer times of heating, this transition may even take place at lower temperatures (Brooker and Nuffield, 1952). In this study a great many diffractometer patterns were taken on pitchblende samples not reported here. Material from at least 15 different localities was examined and, although many of the samples showed impurities, none of the lines of U_3O_8 were seen, although they were carefully looked for. Since it is known that UO_2 can be formed with a stoichiometric excess of oxygen, it is concluded that if U_3O_8 is a stable compound, then none of the pitchblendes examined have been subject to very high temperatures after being deposited and having the reducing environment removed.

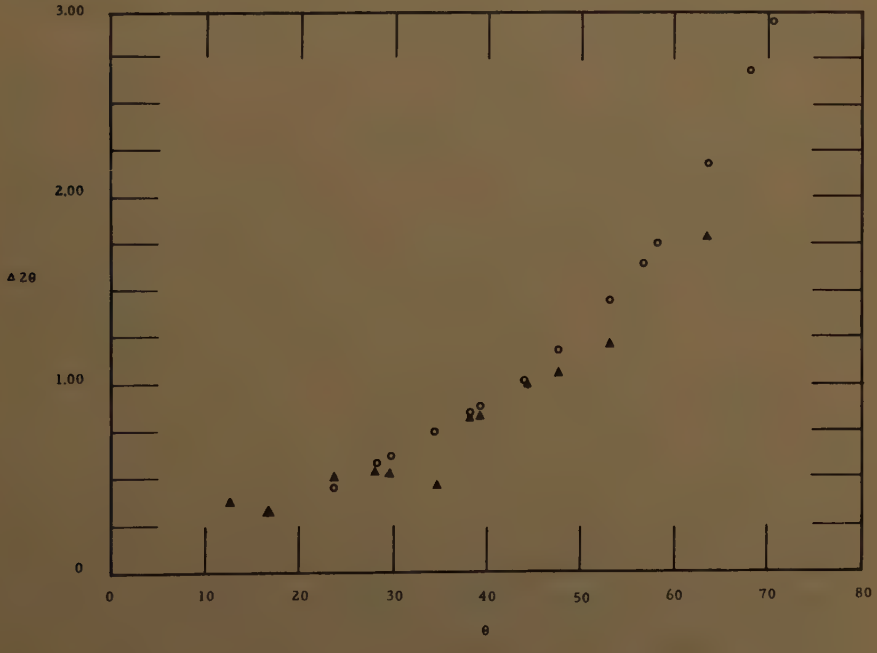

FIGURE 10. Curve to show disorder of uraninite.

Metamict state. The observation of metamict pitchblende has been claimed by Conybeare and Ferguson (1950). Their evidence that the X-ray diffraction patterns of some pitchblendes are sharpened by heating is effectively disputed by Brooker and Nuffield (1952), who show that the heating merely causes a reduction of oxidized UO_2 due to the presence of carbonaceous impurities in the samples. It was proposed to subject some UO_2 to radioactive bombardment to see if disorder could be produced. Although it was never possible to carry out this experiment, due to the lack of facilities, some of the computations involved might be of interest to any worker who may attempt this experiment.

The following computations indicate the quantities of material that would be involved in the X-ray technique currently applied and the α-particle output of a corresponding amount of material in ordinarily recognized periods of geologic time.

The area exposed to X rays is 1 cm. by 2 cm. The depth of penetration of X rays that cuases the maximum diffraction effect may be derived by computation. The linear absorption coefficient μ of UO_2 is determined from $\mu = d\left\{\frac{u}{uo_2}\left(\frac{\mu}{\rho}\right)_u + \frac{o_2}{uo_2}\left(\frac{\mu}{\rho}\right)_o\right\}$ where d is the density and $\frac{\mu}{\rho}$ the mass absorption coefficient obtained from the *International Tables for the Determination of Crystal Structure*. This gives a value of μ on the order of 3×10^3.

The synthetically prepared UO_2 to be used in these experiments has a density of approximately 10. For the sake of these first approximations, the sample is considered to be homogenous solid.

As the depth of penetration of the X rays in the sample t increases, the intensity is decreased according to the absorption law $I = I_o e^{-\mu t}$. At the same time, the diffracted intensity is built up as a function of t^2. Introducing a proportionality constant k, we see that the diffracted intensity $I_{diff} = KI_o e^{-\mu t} t^2$. This net intensity is a maximum when its first derivative with respect to thickness is zero.

$$\frac{dI_{diff}}{dt} = KI_o (e^{-\mu t} \cdot 2t - t^2 \mu e^{-\mu t})$$

$$= KI_o e^{-\mu t} t(2 - t\mu)$$

A maximum is obtained when $2 - t\mu = 0$, e.g., $t = \frac{2}{\mu}$. In this case, $t = .0006$ cm.

The total quantity of sample, assuming a specific gravity of 10, is 12 mg.

For the purpose of computing the α-particle output over a long period of time, we assume secular equilibrium; that is, that the isotope

U^{238} has a half life so much longer than any of its breakdown products that it does not diminish in quantity in the period of time under consideration.

The half life of uranium 238 is about 4.5×10^9 years. The disintegration constant $\lambda = \frac{0.693}{T\ 1/2}$ and has the value 4.9×10^{-18} sec.$^{-1}$

The number of α-particles produced by the given quantity of U^{238} in 10^9 years, which represents some of the older pitchblende samples, is determined as the product of the disintegration constant, the time in seconds, and the number of atoms present.

λ	time	atoms	α/decay
4.9×10^{-18}	10^9 (365) (86,400)	$\frac{.012}{238}(6 \times 10^{23})$	8

This gives a value on the order of 4×10^{19} α-particles.

A number of experimental difficulties exist. In particular, if cyclotron bombardment is used, a large heating effect must be considered. An external beam would have to be used, and the sample would have to be surrounded by an inert gas atmosphere to prevent oxidation and to facilitate heat transfer.

These computations are approximations, and they show only the order of magnitude. The assumptions made seem reasonable, however, *i.e.*, secular equilibrium exists in pitchblende, and only the largest quantity isotope of uranium has been considered. For every uranium atom decay, 8 α-particles are produced.

Note. The use of radium 226 has been considered as a source of α-particles. This has a half life $T\ 1/2 = 1.6 \times 10^3$ years. From this the disintegration constant $\lambda = 1.38 \times 10^{-11}$ sec^{-1} is derived. The product of λ and the number of atoms in one gram of radium 226 gives an α-particle output of 3.6×10^{10} per second or 1.3×10^{14} per hour. Assuming that as much as one tenth of the output could be directed to the sample, one hour's exposure is equivalent to about 10^3 years; 1,000 hours, 100,000 years; and 420 days, 1 million years.

General summary and conclusions. A working usage has been established for the terms uraninite and pitchblende. The term uraninite is reserved for the naturally occurring UO_2 having megascopic crystal size and often showing crystal form, while the term pitchblende is applied to material composed of crystallites on the order of 10^{-3} cm. or less in size. A Laue-type X-ray diffraction diagram made with characteristic radiation may be used to distinguish between these two types. The uraninite produces individual spots characteristic of a single crystal, while pitchblende produces Debye-Scherrer rings characteristic of the microcrystalline aggregate. There does not appear to be any gradation between the macrocrystals and the microcrystalline aggregates.

X-ray examination of the crystal textures of certain boytryoidal pitchblendes shows that the botryoids are composed of parallel fibers whose axes of elongation consist of the poles of the 111 crystal planes. The diffuse diffraction maxima observed from uraninite single crystals is evidence of a disordered structure. This is qualified by analysis of the powder diffraction line broadening data.

A practical method is outlined for determining the true diffraction line breadth from a powdered sample using a Geiger counter diffractometer.

The line broadening of several natural and artificial samples of UO_2 has been determined and, from these, functions have been plotted to indicate the extent of crystallite size line broadening and disorder line broadening.

Two synthetic samples prepared under similar conditions but different temperatures were found to be free from disorder. The sample prepared at the higher temperature has a larger crystallite size. When oxygen is introduced into the system, an appreciable amount of disorder appears, although the crystallite dimension is about the same.

It is observed that, in natural pitchblendes, part of the line broadening is a disorder effect and that, in some cases, it is due to small crystallite dimensions. The elongation of the crystallites in some pitchblendes, as observed by X-ray texture study, is confirmed by the observation that the apparent crystallite dimensions are larger in certain crystallographic directions than in others. Electron micrography of natural pitchblendes does not show this elongation, even though this effect is shown by the synthetic samples.

It is believed that in the case of uraninite, where there is no crystallite size line broadening, the disorder broadening is due to a distribution of unit cells of various sizes. The shape of the diffraction maxima approximates the function representing this distribution. An expression was derived to express the line broadening in terms of Bragg angle, to fit this assumption. A plot of this function alongside a plot of the measured broadening agrees very well.

Acknowledgments. The writer is indebted to Professor Paul F. Kerr of Columbia University, New York, N.Y., under whose guidance this work was carried out.

Specimens for the study were obtained from the mineralogical collections of Columbia University, from the Raw Materials Operations Office of the United States Atomic Energy Commission, Washington, D.C., and through the courtesy of Doctor George Switzer of the United States National Museum, Washington, D.C.

Doctor Frederick Holtzberg of the Watson Scientific Computing

Laboratory of Columbia University was very helpful in allowing the use of the precession camera in his laboratory.

Ronald J. Arnott engaged in conversations with the author which resulted in formulating many of the ideas presented here.

This work was performed under Contract No. AT-30-1-702 for the United States Atomic Energy Commission, Division of Raw Materials.

APPENDICES

Appendix A

Quartz, Brazil
Cu Radiation

1	2	3	4	5	6	7
hkl	2θ	I_{max}	I_{tot}	B°_{raw}	$B_{rad\ raw}$	$B_{rad\ corr}$
100	18.83	1.78	0.25	0.1404	0.00245	0.00245
100	20.85	5.55	1.25	0.2252	0.00393	0.00366
101	24.03	4.08	0.85	0.2083	0.00364	0.00364
110	36.54	5.70	0.94	0.1649	0.00287	0.00209
102	39.47	3.53	0.71	0.2011	0.00351	0.00264
111	40.28	1.80	0.33	0.1833	0.00320	0.00233
121	59.95	1.65	0.38	0.2303	0.00402	0.00279
302	75.64	3.81	1.20	0.3149	0.00549	0.00382
220	77.65	2.17	0.72	0.3317	0.00579	0.00403
131	83.80	2.38	0.80	0.3361	0.00587	0.00403
124	96.25	2.42	0.67	0.2768	0.00483	0.00321
231	106.62	1.75	0.59	0.3371	0.00588	0.00392
134	120.12	2.14	0.71	0.3317	0.00579	0.00376
143	137.88	3.44	1.33	0.3866	0.00675	0.00439
			Rerun			
110	36.56	2.57	0.51	0.1984	0.00346	0.00267
102	39.49	2.49	0.48	0.1927	0.00336	0.00250
112	50.15	3.34	0.70	0.2095	0.00366	0.00259
121	59.97	2.81	0.63	0.2241	0.00391	0.00270

SYNTHETIC UO_2
EXPERIMENT NO. 1
Cu Radiation

1 hkl	2 2θ	3 θ	4 I_{max}	5 I_{tot}	6 B^{o}_{raw}	7 $B_{rad\ raw}$	8 $B_{rad\ corr}$	9 b	10 $\tan\theta$	11 $\cos\theta$	12 $b/\tan\theta$	13 $b\cos\theta$	14 d	15 a_o	16 t
111	28.26	14.13	2.18	0.75	0.344	0.00600	0.00565	0.00292	0.25174	0.96974	0.0116	0.00283	3.1552	5.465	532
200	32.74	16.37	1.12	0.32	0.286	0.00499	0.00447	0.00182	0.29375	0.95946	0.00619	0.00174	2.7329	5.466	898
220	46.98	23.49	4.72	1.70	0.360	0.00628	0.00538	0.00280	0.43460	0.91713	0.00644	0.00257	1.9327	5.466	608
311	55.73	27.86	4.10	1.57	0.382	0.00667	0.00547	0.00279	0.52852	0.88409	0.00527	0.00247	1.6438	5.467	632
222	58.73	29.22	0.78	0.28	0.359	0.00627	0.00495	0.00225	0.55934	0.87275	0.00402	0.00196	1.5778	5.465	798
400	68.61	34.30	0.81	0.28	0.346	0.00604	0.00441	0.00146	0.68215	0.82610	0.00214	0.00121	1.3668	5.467	129
331	75.79	37.89	1.37	0.60	0.438	0.00764	0.00573	0.00273	0.77820	0.78919	0.00350	0.00215	1.2542	5.467	725
331	75.79	37.89	4.58	2.57	0.561	0.00979	0.00803	0.00413	0.77820	0.78919	0.00531	0.00326			478
420	78.13	39.06	3.80	2.18	0.573	0.01002	0.00816	0.00436	0.81152	0.77649	0.00537	0.00339	1.2224	5.467	454
422	87.30	43.65	3.41	2.08	0.610	0.01065	0.00836	0.00481	0.95395	0.72357	0.00504	0.00348	1.1159	5.467	442
333 511	94.11	47.05	3.93	2.34	0.595	0.01038	0.00776	0.00416	1.0742	0.68136	0.00387	0.00283	1.0523	5.468	545
440	105.68	52.85	1.37	0.95	0.693	0.01210	0.00892	0.00527	1.3194	0.60604	0.00399	0.00318	0.96649	5.467	483
531	112.90	56.45	4.18	3.42	0.818	0.01428	0.01060	0.00685	1.5080	0.55266	0.00454	0.00379	0.92422	5.468	406
600 442	115.40	57.70	2.29	1.86	0.812	0.01417	0.01034	0.00656	1.5818	0.53435	0.00415	0.00351	0.91125	5.468	438
620	126.00	63.00	2.71	2.22	0.819	0.01429	0.00997	0.00602	1.9626	0.45399	0.00307	0.00273	0.86447	5.468	566
533	134.98	67.49	1.98	2.14	1.081	0.01887	0.01330	0.00918	2.4130	0.38284	0.00380	0.00351	0.83377	5.467	438
622	138.28	69.14	2.07	2.19	1.058	0.01847	0.01289	0.00869	2.6242	0.35608	0.00331	0.00309	0.82428	5.467	498

SYNTHETIC UO_2
EXPERIMENT NO. 5
Cu Radiation

1 hkl	2 2θ	3 θ	4 I_{max}	5 I_{tot}	6 B^{α}_{raw}	7 $B_{rad\ raw}$	8 $B_{rad\ corr}$	9 b	10 $\tan\theta$	11 $\cos\theta$	12 $b/\tan\theta$	13 $b\cos\theta$	14 d	15 a_o	16 t
111	28.25	14.12	2.10	2.10	1.00	0.01745	0.01731	0.01457	0.25155	0.96979	0.0579	0.0141	3.1574	5.469	109
200	32.80	16.40	0.95	0.78	0.821	0.01433	0.01412	0.01147	0.29431	0.95931	0.0390	0.0110	2.7281	5.456	140
220	47.00	23.50	1.08	1.10	1.0185	0.01777	0.01738	0.01480	0.43481	0.91706	0.0340	0.0136	1.9317	5.463	113
311	55.80	27.90	1.03	1.04	1.0097	0.01762	0.01709	0.01441	0.52947	0.88377	0.0272	0.0127	1.6461	5.460	121
222	58.42	29.21	0.20	0.16	0.8000	0.01396	0.01319	0.01049	0.55911	0.87284	0.0188	0.00915	1.5783	5.467	168
400	68.75	34.37											1.3644	5.458	
331	76.00	38.00	0.38	0.60	1.579	0.02756	0.02673	0.02373	0.02373	0.78801	0.0304	0.0187	1.2511	5.454	82
420	78.30	39.15	0.35	0.43	1.229	0.02145	0.02037	0.01707	0.01707	0.77550	0.0210	0.0132	1.2200	5.456	117
331	75.90	37.95	2.50	3.16	1.264	0.02206	0.02118	0.01728	0.01728	0.78855	0.0222	0.0136	1.2525	5.460	113
420	78.35	39.17	1.95	2.96	1.518	0.02649	0.02570	0.02190	0.02190	0.77528	0.0269	0.0169	1.2195	5.454	91
422	87.52	43.76	2.28	3.36	1.474	0.02573	0.02444	0.02089	0.02089	0.72224	0.0218	0.0151	1.1137	5.456	102
333 511	94.45	47.22	2.30	3.76	1.635	0.02854	0.02711	0.02351	0.02351	0.67919	0.0218	0.0159	1.0494	5.453	97
440	106.00	53.00	0.82	1.13	1.378	0.02405	0.02164	0.01799	0.01799	0.60182	0.0135	0.0108	0.96445	5.456	143
531	113.27	56.63											0.92230	5.456	
600 442	115.60	57.80											0.91025		
620	126.50	63.20	1.35	3.17	2.348	0.04098	0.03791	0.03396	0.03396	0.45088	0.0171	0.0153	0.86294		101
533	135.70	67.80											0.83192		
622	139.00	69.50											0.82232		

SYNTHETIC UO_2
EXPERIMENT NO. [redacted]
Cu Radiation

1 hkl	2 2θ	3 θ	4 I_{max}	5 I_{tot}	6 B°_{raw}	7 $B_{rad\ raw}$	8 $B_{rad\ corr}$	9 b	10 $\tan\theta$	11 $\cos\theta$	12 $b/\tan\theta$	13 $b\cos\theta$	14 d	15 a_o	16 t
111	28.43	14.21	5.46	1.92	0.352	0.00614	0.00580	0.00307	0.2532	0.9694	0.0121	0.00298	3.1378	5.435	516
200	32.97	16.49	2.43	0.81	0.333	0.00581	0.00535	0.00270	0.2960	0.9588	0.0091	0.00259	2.7136	5.427	595
220	47.30	23.65	2.25	0.96	0.427	0.00745	0.00667	0.00409	0.4379	0.9160	0.0093	0.00375	1.9201	5.430	410
311	56.09	28.04	1.93	0.91	0.472	0.00824	0.00721	0.00453	0.5326	0.8826	0.0085	0.00399	1.6385	5.435	382
222	58.86	29.43											1.5676	5.430	
220	47.30	23.65	4.62	1.95	0.422	0.00737	0.00660	0.00402	0.4379	0.9160	0.0092	0.00368	1.9201	5.430	
311	56.12	28.06	3.95	2.00	0.506	0.00883	0.00783	0.00515	0.5330	0.8825	0.0097	0.00454	1.6374	5.431	
222	58.85	29.42	0.97	0.38	0.392	0.00684	0.00557	0.00287	0.5639	0.8710	0.0051	0.00249	1.5681	5.432	
400	69.18	34.59	0.50	0.27	0.540	0.00942	0.00798	0.00503	0.6896	0.8232	0.0073	0.00414	1.3568	5.427	
331	76.32	38.16	1.15	0.71	0.617	0.01077	0.00912	0.00612	0.7858	0.7863	0.0078	0.00481	1.2466	5.434	
420	78.68	39.34	0.95	0.56	0.589	0.01028	0.00845	0.00525	0.8197	0.7734	0.0064	0.00406	1.2151	5.434	
331	76.30	38.15	7.40	5.73	0.774	0.01351	0.01209	0.00819	0.7855	0.7864	0.0104	0.00644	1.2469	5.435	
420	78.62	39.31	6.12	4.62	0.755	0.01318	0.01160	0.00780	0.8188	0.7737	0.0095	0.00603	1.2158	5.437	
422	87.97	43.98	5.23	4.21	0.805	0.01405	0.01208	0.00853	0.9650	0.7196	0.0088	0.00614	1.1092	5.434	
333 511	94.88	47.44	4.90	4.25	0.867	0.01513	0.01286	0.00926	1.0890	0.6764	0.0085	0.00626	1.0457	5.433	
440	106.50	53.20	1.42	1.19	0.838	0.01462	0.01148	0.00783	1.3367	0.5990	0.00585	0.00469	0.9610	5.441	
531	113.90	56.90	4.80	6.20	1.292	0.02255	0.01951	0.01578	1.5340	0.5461	0.0102	0.00861	0.91946	5.439	
600 442	116.50	58.20	2.81	3.44	1.224	0.02136	0.01794	0.01416	1.6128	0.5269	0.00878	0.00746	0.90628	5.438	
620	127.30	63.60	2.25	3.14	1.395	0.02437	0.01986	0.01591	2.0145	0.4446	0.00789	0.00707	0.85993	5.439	
533	136.70	68.30	1.90	3.67	1.931	0.03370	0.02854	0.02442	2.5129	0.3697	0.00971	0.00903	0.82900	5.436	
622	140.20	70.10	1.85	3.47	1.876	0.03274	0.02717	0.02297	2.7624	0.3404	0.00831	0.00782	0.81916	5.433	

URANINITE (SINGLE CRYSTAL, POWDERED)
SHINKOLOBWE, BELGIAN CONGO
Cu Radiation

1 hkl	2 2θ	3 θ	4 I_{max}	5 I_{tot}	6 B°_{raw}	7 $B_{rad\ raw}$	8 $B_{rad\ corr}$	9 b	10 $\tan\theta$	11 $\cos\theta$	12 $b/\tan\theta$	13 $b\cos\theta$	14 d	15 a_o
111	25.58	12.79	1.70	0.57	0.335	0.00584	0.00584	0.00304	0.2270	0.9752	0.0134	0.00296		
111	28.34	14.17	5.73	2.22	0.387	0.00675	0.00645	0.00375	0.2525	0.9696	0.0148	0.00364	3.1464	5.4495
200	29.60	14.80	0.54	0.15	0.277	0.00483	0.00483	0.00213	0.2642	0.9668	0.00806	0.00206		
200	32.85	16.42	2.35	0.81	0.345	0.00602	0.00557	0.00292	0.2947	0.9592	0.00991	0.00280	2.7248	5.4496
111	28.34	14.17	8.40										3.1464	5.4495
200	32.88	16.44	3.15	1.13	0.359	0.00627	0.00583	0.00318	0.2951	0.9591	0.0107	0.00305	2.7216	5.443
220	47.18	23.59	3.20	1.77	0.553	0.00965	0.00899	0.00641	0.4367	0.9164	0.0147	0.00587	1.9247	5.443
311	55.95	27.97	2.50	1.59	0.636	0.01110	0.01027	0.00759	0.5310	0.8832	0.0143	0.00670	1.6423	5.447
222	58.70	29.35	0.60	0.35	0.583	0.01017	0.00915	0.00645	0.5623	0.8716	0.0114	0.00562	1.5715	5.443
400	68.87	34.43	0.65	0.35	0.538	0.00939	0.00791	0.00491	0.6855	0.8248	0.00716	0.00405	1.3623	5.449
331	76.13	38.06	1.50	1.18	0.787	0.01373	0.01229	0.00929	0.7827	0.7874	0.0118	0.00731	1.2494	5.446
420	78.35	38.17	1.05	0.83	0.790	0.01379	0.01225	0.00925	0.8147	0.7753	0.0113	0.00717	1.2195	5.454
422	87.71	43.85	5.60	6.41	1.145	0.01998	0.01848	0.01488	0.9606	0.7212	0.0154	0.01073	1.1118	5.447
333 511	94.60	47.30	5.05	5.90	1.168	0.02038	0.01855	0.01495	1.0830	0.6782	0.0138	0.01014	1.0481	5.446
440	106.25	53.12	1.68	2.23	1.327	0.02316	0.02080	0.01715	1.3330	0.6001	0.0129	0.01029	0.96294	5.447
620	126.90	63.45	2.40	4.34	1.808	0.03155	0.02767	0.02372	2.0010	0.4469	0.0119	0.01060	0.86105	5.446
533	136.10	68.00											0.8307	5.446
622	139.30	69.60											0.8218	5.451
422	87.70	43.85	4.20	4.87	1.595	0.02783	0.02663	0.02303	0.9606	0.7212	0.0239	0.01660	1.1118	5.447
333 511	94.55	47.27	3.90	4.45	1.141	0.01991	0.01796	0.01436	1.0820	0.6785	0.0132	0.00974	1.0486	5.448
440	106.30	53.10	1.30	1.73	1.331	0.02323	0.02090	0.01725	1.3310	0.6004	0.0129	0.01035	0.9632	5.449
531	113.60	56.80											0.9205	5.446
600 442	116.10	58.50											0.9034	5.420
620	126.90	63.40	1.80	3.58	1.989	0.03471	0.03107	0.02712	0.02712	0.4478	0.0136	0.01214	0.8614	5.448
533	136.10	68.00											0.8307	5.447
622	139.30	69.60											0.8218	5.451

PITCHBLENDE,
HAPPY JACK MINE, MONTICELLO, UTAH
Cu Radiation

1	2	3	4	5	6	7	8	9	10	11	12	13	14	15	16
hkl	2θ	θ	I_{max}	I_{tot}	B°_{raw}	$B_{rad\ raw}$	$B_{rad\ corr}$	b	$\tan\theta$	$\cos\theta$	$b/\tan\theta$	$b\cos\theta$	d	a_o	t
111	25.57		0.85	0.29	0.341	0.005951	0.00595								
111	28.59	14.29	3.28	1.56	0.476	0.008307	0.00805	0.00531	0.2547	0.9690	0.0208	0.00514	3.1206	5.405	300
200	29.82														
200	33.13	16.56	1.32	0.61	0.462	0.008063	0.00769	0.00504	0.2973	0.9585	0.0169	0.00483	2.7024	5.405	319
111	28.58	14.29	2.69	1.38	0.513	0.008954	0.00870	0.00596	0.2547	0.9690	0.0234	0.00578	3.1206	5.405	266
200	33.12	16.56	1.02	0.47	0.461	0.008045	0.00772	0.00507	0.2973	0.9585	0.0170	0.00486	2.7024	5.405	317
220	47.59	23.79	2.10	1.31	0.624	0.010890	0.01032	0.00774	0.4408	0.9150	0.0175	0.00708	1.9095	5.400	218
311	56.42	28.21	1.72	1.12	0.651	0.011362	0.01056	0.00788	0.5364	0.8812	0.0147	0.00694	1.6294	5.405	
222	59.17	29.58	0.35	0.18	0.514	0.008971	0.00787	0.00517	0.5676	0.8696	0.0091	0.00449	1.5603	5.405	
400	69.60	34.80											1.3496	5.398	
331	76.85	38.42	1.67	1.59	0.952	0.016615	0.01536	0.01151	0.7932	0.7834	0.0145	0.00901	1.2395	5.403	
420	79.25	39.62	1.32	1.31	0.992	0.017313	0.01601	0.01223	0.8279	0.7703	0.0147	0.00942	1.2079	5.402	
422	88.65	44.32	1.14	1.13	0.991	0.017296	0.01556	0.01196	0.9765	0.7154	0.0122	0.00856	1.1025	5.401	
333 511	95.67	47.83	1.10	1.07	0.972	0.016964	0.01475	0.01115	1.1040	0.6713	0.0101	0.00748	1.0393	5.400	
440	107.50	53.70	0.40	0.55	1.375	0.023998	0.02171	0.01804	1.3613	0.5920	0.0133	0.01067	0.95573	5.406	
531	115.10	57.55	1.20	1.87	1.558	0.027192	0.02447	0.02069	1.5727	0.5366	0.0132	0.01163	0.91277	5.400	
600 442	117.60	58.80	0.72	1.06	1.472	0.025691	0.02260	0.01880	1.6511	0.5180	0.0114	0.00973	0.90049	5.403	
620	128.90	64.40	0.55	0.81	1.472	0.025691	0.02080	0.01680	2.0871	0.4320	0.0080	0.00725	0.85409	5.402	
533	138.60	69.80	0.47	0.94	2.000	0.034907	0.02879	0.02459	2.7179	0.3453	0.0090	0.00849	0.82072	5.381	
622	142.20	71.10	0.45	1.12	2.489	0.043441	0.03801	0.03371	2.9207	0.3239	0.0115	0.01091	0.81414	5.400	

PITCHBLENDE
HUMMELFURST, SAXONY
Cu Radiation

1 hkl	2 2θ	3 θ	4 I_{max}	5 I_{tot}	6 B°_{raw}	7 $B_{rad\ raw}$	8 $B_{rad\ corr}$	9 b	10 $\tan\theta$	11 $\cos\theta$	12 $b/\tan\theta$	13 $b\cos\theta$	14 d	15 a_o	16 t
111	25.70	12.85	0.65	0.37	0.569	0.00993									
111	28.57	14.29	2.35	1.67	0.711	0.01241	0.01222	0.00952	0.2547	0.9690	0.0373	0.00922			167
200	33.08	16.54	0.80	0.58	0.725	0.01265	0.01242	0.00977	0.2969	0.9586	0.0329	0.00936			165
111	25.70	12.85	0.70	0.39	0.557	0.00972									
111	28.53	14.26	2.45	1.82	0.742	0.01295	0.01278	0.01008	0.2541	0.9691	0.0397	0.00976			158
200	33.05	16.52	0.85	0.58	0.682	0.01190	0.01166	0.00901	0.2966	0.9587	0.0304	0.00863			178
111	28.55	14.27	4.35	3.08	0.708	0.01235	0.01216	0.00946	0.2543	0.9691	0.0372	0.00917			168
200	33.08	16.54	1.52	1.07	0.704	0.01228	0.01205	0.00940	0.2969	0.9586	0.0317	0.00901			171
220	47.50	23.75	1.35	1.24	0.918	0.01602	0.01565	0.01310	0.4400	0.9153	0.0297	0.01199			128
311	56.40	28.20	1.05	1.20	1.142	0.01993	0.01963	0.01693	0.5362	0.8813	0.0315	0.01492			103
222	59.00	29.50													
400	69.30	34.70													
331	76.80	38.40													
420	79.03	39.52													
422	88.30	44.10	1.30	2.43	1.869	0.03252	0.03165	0.02805	0.9690	0.7181	0.0289	0.02014			
333 511	95.25	47.62	1.20	1.96	1.633	0.02850	0.02710	0.02350	1.0959	0.6740	0.0214	0.01583			
531	114.50														
600 442	116.00														
620 533 620	128.50	64.20	0.55	1.53	2.781	0.04586	0.04586	0.04186	2.0686	0.4352	0.0202	0.01821			

PITCHBLENDE, RICKARDS MINE, GILPIN CO., COLO.
Cu Radiation

1 hkl	2 2θ	3 θ	4 I_{max}	5 I_{tot}	6 B°_{raw}	7 $\beta_{rad\ raw}$	8 $\beta_{rad\ corr}$	9 b	10 $b/\tan\theta$	11 $b\cos\theta$	12 $\sin\theta$	13 I
111	25.60	12.80	1.51	0.86	0.558	0.00974	0.00956	0.00676	0.0297	0.00659	0.2215	
111	28.42	14.21	5.98								0.2454	
200	32.95	16.47	2.35	1.39	0.591	0.01031	0.01004	0.00744	0.0252	0.30713	0.2835	215
	42.50											
220	47.40	23.70	2.35	1.99	0.846	0.01477	0.01434	0.01174	0.0267	0.01074	0.4019	143
	50.30											
311	56.23	28.11	1.70	1.82	1.071	0.01869	0.01818	0.01548	0.0289	0.01365	0.4711	112
422	88.20	44.10	1.50	3.17	2.11	0.03682	0.03597	0.03237	0.0334	0.02324	0.6959	66
511	95.10	47.50	1.30	2.60	2.00	0.03491	0.03393	0.03033	0.0277	0.02045	0.7372	75
333												

Appendix B

Line Breadth Increase Due to $\frac{\Delta a}{a_o}$

$a_o = 5.447$

$\frac{\Delta a}{a_o} = 0.00947$

	$a_1 = 5.4724$		$a_2 = 5.4208$				Uraninite Belgian Congo
hkl	da_1	θ_1	da_2	θ_2	$\Delta\theta$	$\Delta 2\theta$	$\Delta 2\theta$
111	3.1761	14.04	3.1298	14.25			.369
200	2.7362	16.35	2.7104	16.51	.16	.32	.319
220	1.9351	23.46	1.9168	23.69	.23	.46	.515
311	1.6498	27.83	1.6342	28.12	.29	.58	.588
222	1.5798	29.18	1.5649	29.49	.31	.62	.524
400	1.3681	34.26	1.3552	34.64	.38	.76	.453
331	1.2554	37.85	1.2436	38.27	.42	.84	.704
420	1.2237	39.01	1.2122	39.45	.44	.88	.702
422	1.1170	43.60	1.1065	44.11	.51	1.02	1.058
333-511	1.0532	47.00	1.0433	47.59	.59	1.18	1.063
440	.96737	52.77	.95825	53.49	.72	1.44	1.192
531	.92502	56.38	.91629	57.20	.82	1.64	
600-442	.91207	57.62	.90347	58.49	.87	1.74	
620	.86520	62.90	.85704	63.99	1.09	2.18	1.78
533	.83459	67.36	.82672	68.70	1.34	2.68	
622	.82503	69.00	.81725	70.47	1.47	2.94	

References

Bragg, W. L. 1933. The Crystalline State. Bell and Sons. London, England.

Brill, R. 1928. Teilchengrössenbestimmungen mit Hilfe von Röntgenstrahlen. Z. Krist. **68**: 387-403.

Brooker, E. J. & E. W. Nuffield. 1952. Studies of radioactive compounds: IV - Pitchblende from Lake Athabaska, Canada. Am. Mineralogist. **37**: 363.

Conybeare, C. E. B. & R. B. Ferguson. 1950. Metamict pitchblende from Goldfields, Saskatchewan and observations on some ignited pitchblendes. Am. Mineralogist. **35**: 401.

Davidson, C. F. & S. H. U. Bowie. 1951. On thucholite and related hydrocarbon-uraninite complexes. Bull. Geol. Survey Gt. Brit. No. 3: 1.

Ellsworth, H. V. 1932. Rare element minerals of Canada. Geol. Survey Can., Econ. Geol. Ser. **11**.

Jones, F. W. 1938. The measurement of particle size by the X-ray method. Proc. Roy. Soc. London. (A)**166**: 16-43.

Katz, J. J. & E. Rabinowitch. 1951. The Chemistry of Uranium. Pt. 1. McGraw-Hill. New York, N. Y.

Kerr, P. F. 1950. Mineralogical studies of uraninite and uraninite-bearing deposits. U. S. Atomic Energy Comm. Interim Technical Report.

Kochendorfer, A. 1937. Rontgenographische Teilchengrössenbestimmung an Blechen. Z. Krist. **97**: 469-475.

Niedzwiedzki, J. 1909. Centralblatt fur Min. Geol. u. Paleontol.: 661-663.

Palache, C., H. Berman & C. Frondel. 1944. Dana's System of Mineralogy. 7th ed. 1. New York, N. Y.

ROGERS, A. F. 1947. Uraninite and pitchblende. Am. Mineralogist. **32**: 90.

SCHERRER, P. 1918. Bestimmung der Grosse u. der inneren Struktur von Kolloidteilchen mittels Röntgenstrahlen. Nachr. Ges. Wiss. Göttingen, Zitzunsber. *See:* R. ZSIGMONDY. 1920. Kolloidchemie. 3rd ed. Spamer. Leipzig, Germany.

VON LAUE, M. 1926. Lorentz-Faktor u. Intensitätsverteilung in Debye-Scherrer-Ringen. Z. Krist. **64**: 116. Pt. II, Pulver aus sehr kleinen Kristallteilchen die Maxima der Interferenzfunktion haben merkliche Breite.

YAGODA, H. 1946. The localization of uranium and thorium minerals in polished sections. Am. Mineralogist. **31**: 92.

Printed in the United States of America

MONOGRAPHIC PUBLICATIONS
OF
THE NEW YORK ACADEMY OF SCIENCES

(LYCEUM OF NATURAL HISTORY, 1817–1876)

(1) The ANNALS (octavo series), established in 1823, contain the scientific contributions and reports of researches, together with the records of meetings of the Academy. The articles which comprise each volume are printed separately, each in its own cover, and are distributed immediately upon publication. The price of the separate articles depends upon their length and the number of illustrations, and may be ascertained upon application to the Executive Director of the Academy.

Current numbers of the ANNALS are sent free to all members of the Academy desiring them.

(2) The SPECIAL PUBLICATIONS established in 1939, are issued at irregular intervals as cloth-bound volumes. The price of each volume will be advertised at time of issue.

(3) The MEMOIRS (quarto series), established in 1895, are issued at irregular intervals. It is intended that each volume shall be devoted to monographs relating to some particular department of science. Volume I, Part 1, is devoted to Astronomical Memoirs, Volume II to Zoological Memoirs. No more parts of the Memoirs have been published to date. The price is one dollar per part.

(4) The SCIENTIFIC SURVEY OF PORTO RICO AND THE VIRGIN ISLANDS (octavo series), established in 1919, gives the detailed reports of the anthropological, botanical, geological, paleontological, zoological, and meteorological surveys of these islands.

Subscriptions and inquiries concerning current and back numbers of any of the publications of the Academy should be addressed to

EXECUTIVE DIRECTOR
The New York Academy of Sciences
2 East Sixty-third Street
New York 21, N. Y.